ORIGINAL ARTICLE

JBMR®

Bicarbonate Recycling by HIF-1–Dependent Carbonic Anhydrase Isoforms 9 and 12 Is Critical in Maintaining Intracellular pH and Viability of Nucleus Pulposus Cells

Elizabeth S Silagi,[1,2] Zachary R Schoepflin,[1,2] Erin L Seifert,[1,3] Christophe Merceron,[4] Ernestina Schipani,[4,5] Irving M Shapiro,[1,2] and Makarand V Risbud[1,2]

[1]Program in Cell Biology and Regenerative Medicine, Jefferson College of Biomedical Sciences, Thomas Jefferson University, Philadelphia, PA, USA
[2]Department of Orthopaedic Surgery, Sidney Kimmel Medical College, Thomas Jefferson University, Philadelphia, PA, USA
[3]MitoCare Center, Department of Pathology, Anatomy and Cell Biology, Thomas Jefferson University, Philadelphia, PA, USA
[4]Department of Orthopaedic Surgery, University of Michigan Medical School, Ann Arbor, MI, USA
[5]Department of Medicine, Division of Endocrinology, University of Michigan Medical School, Ann Arbor, MI, USA

ABSTRACT

Intervertebral disc degeneration is a ubiquitous condition closely linked to chronic low-back pain. The health of the avascular nucleus pulposus (NP) plays a crucial role in the development of this pathology. We tested the hypothesis that a network comprising HIF-1α, carbonic anhydrase (CA) 9 and 12 isoforms, and sodium-coupled bicarbonate cotransporters (NBCs) buffer intracellular pH through coordinated bicarbonate recycling. Contrary to the current understanding of NP cell metabolism, analysis of metabolic-flux data from Seahorse XF analyzer showed that CO_2 hydration contributes a significant source of extracellular proton production in NP cells, with a smaller input from glycolysis. Because enzymatic hydration of CO_2 is catalyzed by plasma membrane-associated CAs we measured their expression and function in NP tissue. NP cells robustly expressed isoforms CA9/12, which were hypoxia-inducible. In addition to increased mRNA stability under hypoxia, we observed binding of HIF-1α to select hypoxia-responsive elements on CA9/12 promoters using genomic chromatin immunoprecipitation. Importantly, in vitro loss of function studies and analysis of discs from NP-specific HIF-1α null mice confirmed the dependency of CA9/12 expression on HIF-1α. As expected, inhibition of CA activity decreased extracellular acidification rate independent of changes in HIF activity or lactate/H^+ efflux. Surprisingly, CA inhibition resulted in a concomitant decrease in intracellular pH that was mirrored by inhibition of sodium-bicarbonate importers. These results suggested that extracellular bicarbonate generated by CA9/12 is recycled to buffer cytosolic pH fluctuations. Importantly, long-term intracellular acidification from CA inhibition lead to compromised cell viability, suggesting that plasma-membrane proton extrusion pathways alone are not sufficient to maintain homeostatic pH in NP cells. Taken together, our studies show for the first time that bicarbonate buffering through the HIF-1α–CA axis is critical for NP cell survival in the hypoxic niche of the intervertebral disc. © 2017 American Society for Bone and Mineral Research.

KEY WORDS: CELL/TISSUE SIGNALING–TRANSCRIPTION FACTORS; CHONDROCYTE AND CARTILAGE BIOLOGY; INTERVERTEBRAL DISC; NUCLEUS PULPOSUS; CARBONIC ANHYDRASE; PH REGULATION; HIF-1

Introduction

Low back pain (LBP) is the leading cause of years lived with disability in the United States and the second leading cause of disability-adjusted life years.[1,2] LBP is caused by dysregulation and degeneration of the core structures of the spinal column: vertebrae and intervertebral disc. The disc comprises an outer fibrocartilaginous annulus fibrosus (AF), surrounding a gelatinous notochord-derived nucleus pulposus (NP), and cartilaginous endplates on the superior and inferior junctions with the vertebral bodies.

Due to a lack of tissue vasculature, cells of the NP reside in a unique hypoxic, acidic, and nutrient-limiting environment.[3–6] Oxygen and nutrients diffuse from vasculature in the surrounding vertebrae, through the cartilaginous endplates and NP cell matrix, to reach the NP cells in the center of the disc. Metabolites cross the reverse path to be cleared from the NP compartment. Given that NP cells reside in a physiologically hypoxic niche and rely primarily on glycolysis for ATP generation, it is thought that these cells produce lactic acid which contributes to their acidic milieu.[7–10] NP cells have a relatively low intracellular pH (pH_i) (measured at 6.7 in bovine cells) and studies suggest that the extracellular pH during degeneration can fall below 6.5.[11–13] Importantly, with degeneration, poor solute clearance through sclerotic endplates coupled with a drop in pH_i may create an environment that predisposes NP cells to considerable cellular

Received in original form April 27, 2017; revised form August 18, 2017; accepted September 6, 2017. Accepted manuscript online September 22, 2017.
Address correspondence to: Makarand V Risbud, PhD, Department of Orthopaedic Surgery, Sidney Kimmel Medical College, Thomas Jefferson University, Philadelphia, PA 19107, USA. E-mail: Makarand.risbud@jefferson.edu
Additional Supporting Information may be found in the online version of this article.
Journal of Bone and Mineral Research, Vol. 33, No. 2, February 2018, pp 338–355
DOI: 10.1002/jbmr.3293

stress. Pathologically acidic pH in NP cells has been shown to lead to matrix catabolism and decreased glucose uptake.[14–16]

NP cells must therefore rely on robust pH-regulating systems to maintain the optimal pH for cellular metabolism, matrix production, and survival. It is widely accepted that pH regulation involves membrane-associated ion transporters and cytosolic as well as plasma membrane-associated carbonic anhydrases (CAs) to sense and balance levels of H^+, HCO_3^-, and CO_2. However, the pH_i regulating capabilities of NP cells, including both plasma membrane H^+-extrusion and HCO_3^- buffering pathways (including pathways of CO_2 production), are largely unexplored. In regard to H^+ extrusion, a study has detected the presence of Na^+/H^+ exchangers and H^+-ATPases in NP cells that both enable H^+ efflux as a means of regulating pH_i.[11] On the other hand, the mechanisms contributing to HCO_3^- buffering in NP cells remain unknown.

The general model of pH_i regulation via the HCO_3^- buffering capabilities of carbonic anhydrases is extensively studied in other cell types.[17–22] CAs are a family of 16 proteins which catalyze the reversible hydration of CO_2 to produce equal parts HCO_3^- (basic) and H^+ (acidic) units at an exceedingly efficient rate of up to $1 \times 10^6\ s^{-1}$ at 37°C.[23] However, the specific function of the various isoforms is not redundant; their functional relevance is determined by cellular localization (plasma membrane versus cytosol versus mitochondrial membrane) and the directionality of the enzymatic reaction (favoring production of HCO_3^-/H^+ or CO_2/H_2O). In fact, contrary to the general understanding, rates of CO_2 hydration by CAs are substantial enough to contribute up to 100% of total extracellular proton production, a metric often erroneously associated solely with glycolytic lactate/H^+ production.[24] Interestingly, our published RNA-Seq (GEO Accession #GSE86552) and microarray data (#GSE42611) along with other expression studies (GSE49560, GSE24612) show that levels of CA9, CA12, and CA3 expression are the highest in rat NP cells.[25–28] These studies also show that NP cells express CA2 (cytosolic) and CA5b (mitochondrial) at lower levels, whereas the remaining CA isoforms were undetectable.

Recently it has been found that the membrane-associated and extracellularly facing CA9 and CA12 isoforms are rapidly induced by hypoxia inducible factor-1α (HIF) under hypoxic conditions in select cell types.[29–31] Although these isoforms show broader expression in embryonic tissues, their expression is restricted to few adult tissues and elevated in hypoxic tumors.[32,33] In cancer cells, they are shown to be robust pH_i regulators by generating HCO_3^- that is recycled into the cell through the coordinated actions of HCO_3^- transporters, which include the SLC4 and SLC26 families of proteins.[20,34] The electrogenicity and directionality of HCO_3^- transport is varied for each isoform. However, important to this work, the Na^+-coupled/HCO_3^- cotransporters (NBCs) are all capable of bicarbonate influx and are sensitive to inhibition by the Stilbene derivative, Stilbene-isothiocyanate–sulfonic acid (SITS).[35]

NP cells adapt to their unique hypoxic environment through the essential activities of the HIF homologues,[4] which are regulated in a unique fashion in the NP.[5,36–40] HIF-1α, in particular, regulates the expression of many genes critical to the survival of NP cells—including enzymes controlling glycolysis.[10] Likewise, HIF-1 is implied to control CA12 expression in NP cells; however, in vivo evidence and mechanistic insights of this regulation are lacking.[41,42] We hypothesize that the HIF-1α–CA9/12 axis is critical for pH_i regulation in NP cells. We clearly show that the inhibition of CA9 and CA12 in NP cells not only leads to decreased extracellular acidification rate (ECAR), but also pH_i, implying a contribution to extracellular HCO_3^- generation and its cytosolic retrieval through NBCs. Importantly, long-term cytosolic acidification of NP cells due to catalytic inhibition of CA9 and CA12 results in increased incidence of cell death. Taken together, our studies show for the first time that bicarbonate buffering through the HIF-1α–CA axis is critical for NP cell survival in the hypoxic niche of the intervertebral disc.

Materials and Methods

Isolation of NP cells, cell treatments and hypoxic culture

Rat NP cells were isolated and characterized as reported.[4] Cells were maintained in Dulbecco's Modification of Eagle's Medium (DMEM) and 10% FBS supplemented with antibiotics. To investigate the effects of carbonic anhydrase inhibition, cells were treated with acetazolamide (AZA; 100 nM, 500 nM), methazolamide (MZA; 500 nM), and U-104 (500 nM, 2 μM) for 18 hours after 24-hour pretreatment in hypoxia. MZA and AZA are pan-CA inhibitors, whereas U-104 was designed to specifically inhibit CA9/12. It is selective for CA9 and CA12 (inhibitory constant [K_i] = 45 nM and 4.5 nM, respectively) with very low inhibition for CA1 and CA2 (K_i = 5080nM and 9640nM, respectively).[43] Cells were cultured in a hypoxia workstation (Invivo2 300; Baker Ruskinn, Bridgend, UK) with a mixture of 1% O_2, 5% CO_2, and 94% N_2. To investigate the effect of NBC inhibition, we treated NP cells with SITS (100 μM, 250 μM, and 500 μM) for 18 hours after 24-hour pretreatment in hypoxia. To investigate the effect of HIF-1α stabilization on CA9/12 expression under normoxia, we inhibited prolyl hydroxylase (PHD) activity with dimethyloxalylglycine (DMOG) (2 mM) for 8 and 24 hours.

Seahorse XF analyzer respiratory assay

The Seahorse XF24 instrument (Agilent Technologies, Santa Clara, CA, USA) was used to measure ECAR and O_2 consumption rate (OCR), as reported by Csordás and colleagues.[44] Rat NP cells were seeded on a 24-well XF Analyzer plate at 15,000 cells per well. Cells were incubated in hypoxia for 24 hours prior to treatment with three carbonic anhydrase inhibitors for 18 hours and new assay media was added (DMEM, 5 mM glucose, 4 mM glutamine, pH 7.4 at 37°C). While the microplate was incubating for 1 hour at 37°C, no CO_2 and in normoxia, the antimycin-filled sensor cartridge was loaded into the Seahorse XF Analyzer for calibration. The assay protocol was a repeated sequence of 2 min mix, 2 min wait, and 2 min measurement. The measurement phase involves the lowering of the probe array to create a minimally oxygen-impermeable microchamber that allows amplification of O_2 changes due to cellular processes. The OCR was calculated using the Akos algorithm, a standard algorithm which we determined was appropriate even for the low OCR readings that we recorded in NP cells; appropriateness was based on the approximate linearity of the pO_2 versus time traces. ECAR was measured from readings of H^+ concentration. After each measurement, the probe array rises, after which the solution in each well was mixed for 2 min (by gently moving the probe array up and down) to remove O_2 and metabolite gradients, followed by a 2-min waiting period before the next measurement phase (ie, lowering of the probe). Our experiments included eight OCR and ECAR measurements to create a baseline, followed by the injection of Antimycin A (Sigma-Aldrich, St. Louis, MO, USA). Three OCR and ECAR measurements

were then made. All measurements were normalized to total protein concentration using a standard bicinchoninic acid (BCA) assay. Mitochondrial OCR was calculated by subtracting the final OCR value (pmol O_2/min) after Antimycin A treatment from the average of the three OCR values before Antimycin A treatment. In a separate assay, cells were treated with oligomycin; carbonyl cyanide, 4-trifluoromethoxyphenylhydrazone (FCCP) (200 nM, 400 nM, 800 nM, and 1000 nM); and Antimycin A to determine total electron transport chain capacity.

Real-time RT-PCR analysis

Total RNA was extracted from NP cells using RNAeasy mini columns (Qiagen, Valencia, CA, USA). Before elution from the column, RNA was treated with RNase-free DNase I (Qiagen). Purified, DNA-free RNA was converted to cDNA using EcoDry Premix (Clontech Laboratories, Palo Alto, CA, USA). Template cDNA and gene-specific primers were added to the SYBR Green master mixture (Applied Biosystems, Foster City, CA, USA) and mRNA expression was quantified using the Step One Plus Real-time PCR System (Applied Biosystems). Hypoxanthine-Guanine Phosphoribosyltransferase 1 (HPRT) was used to normalize gene expression. Melting curves were analyzed to verify the specificity of the RT-PCR and the absence of primer dimer formation. Each sample was analyzed in duplicate and included a template-free control. All primers used were synthesized by Integrated DNA Technologies, Inc. (Coralville, IA, USA).

Actinomycin D chase analysis

To assess mRNA stability, cells were treated with Actinomycin D (5 μg/mL) for 0, 4, 8, and 24 hours. Total RNA was extracted from cells as described in the Real-time RT-PCR analysis method section. Relative mRNA expression was quantified and data were fit to a regression curve to calculate the mRNA half-life ($t_{1/2}$) of Car9 and Car12 genes under normoxic and hypoxic culture conditions.

Protein extraction, immunoprecipitation, and Western blotting

Cells were placed on ice immediately following treatment and washed with ice-cold PBS. Wash buffer and lysis buffer contained 1× protease inhibitor cocktail (Thermo Fisher Scientific, Waltham, MA, USA), NaF (4 mM), Na_3VO_4 (20 mM), NaCl (150 mM), β-glycerophosphate (50 mM), and dithiothreitol (DTT) (0.2 mM). Total cell proteins were resolved on 10% SDS-polyacrylamide gels and transferred to polyvinylidene fluoride (PVDF) membranes (Fisher Scientific, Pittsburgh, PA, USA). Membranes were blocked with 5% nonfat dry milk in TBST (50 mM Tris, pH 7.6, 150 mM NaCl, 0.1% Tween-20) and incubated overnight at 4°C in 5% nonfat dry milk in TBST with the anti-HIF-1α (1:500; R&D Systems, Minneapolis, MN, USA); anti-CAIX (1:1000; Novus Biologicals, Littleton, CO, USA), anti-CAXII (1:1000; Cell Signaling Technology, Beverly, MA, USA), anti-MCT4 (1:1000; Novus Biologicals), or anti-β-tubulin (1:5000, Developmental Studies Hybridoma Bank [DSHB], Iowa City, IA, USA) antibodies. Specificity of all antibodies has been validated by the manufacturers using siRNA or negative control IgG. Immunolabeling was detected using enhanced chemiluminescence (ECL) reagent (LAS4000; GE Life Sciences). Densitometric analysis was performed using ImageQuant TL (GE Healthcare Life Sciences, Marlborough, MA, USA).

Immunohistological analysis

Seventeen-week-old mouse tails were harvested and fixed in 4% paraformaldehyde (PFA) for 24 hours and decalcified in 12.5% EDTA at 4°C for 6 weeks prior to paraffin embedding. Coronal sections, 7 μm in thickness, were deparaffinized, rehydrated through graded alcohols, and antigens were retrieved with citrate buffer pH 6 for 20 min. Slides were blocked in 5% normal donkey serum in PBST (1× PBS, 0.4% Triton-X) for 1 hour at room temperature. Sections were then sequentially incubated with antibodies carbonic anhydrase IX (CAIX) (1:500; Novus Biologicals) and carbonic anhydrase XII (CAXII) (1:500; Cell Signaling Technology) with an NP marker, Keratin 19 (DSHB product TROMA-III; 1:3; DSHB), a in 5% normal donkey serum in PBST at 4°C overnight.[45] After thoroughly washing the sections, the bound primary antibodies were incubated with Alexa Fluor-594 AffiniPure F(ab′)2 conjugated anti-rabbit or anti-rat secondary antibodies (Jackson ImmunoResearch, West Grove, PA, USA) for 1 hour at room temperature. Sections were visualized using a fluorescence microscope (AxioImager A2; Zeiss, Inc., Thornwood, NY, USA) fitted with a monochromatic camera (AxioCam MRm; Zeiss).

Generation of NP-specific HIF-1α knockout mice

NP-specific HIF-1α knockout mice were generated by the strategy reported by Merceron and colleagues[46] in 2014. Briefly, $Foxa2^{Cre}$ knock-in males were bred with homozygous HIF-1α floxed ($HIF\text{-}1\alpha^{f/f}$) females to generate heterozygous floxed $Foxa2^{Cre}$;$HIF\text{-}1\alpha^{f/+}$ animals. Heterozygous males ($Foxa2^{Cre}$;$HIF\text{-}1\alpha^{f/+}$) were crossed with homozygous floxed $HIF\text{-}1\alpha^{f/f}$ females to generate $Foxa2^{Cre}$;$HIF\text{-}1\alpha^{f/f}$ mutant mice, $Foxa2^{Cre}$;$HIF\text{-}1\alpha^{f/+}$, and $HIF\text{-}1\alpha^{f/f}$ control mice. Embryos were collected at embryonic day 15.5 (E15.5), sectioned and immunostained as described in the Immunohistological analysis method section. CAIX/CAXII staining intensity density was quantified using Fiji (ImageJ) Software (ImageJ; NIH, Bethesda, MD, USA; https://imagej.nih.gov/ij/). A region of interest was specifically drawn to include only the NP tissue compartment; staining intensity was determined by measuring integrated density per area.

Plasmids and reagents

LV-shHIF-1α (#232222 designated clone 1, #54450 designated clone 2) and control pLKO.1 were purchased from Sigma-Aldrich. The following plasmids were obtained from the Addgene repository: HRE-Luc (#26731) developed by Navdeep Chandel; psPAX2 (catalogue no. 12260); and pMD2G (catalogue no. 12259) developed by Dr. Didier Trono.

Lentiviral particle production and viral transduction

HEK293T cells were seeded in 10-cm plates (1.3×10^6 cells/plate) in Opti-MEM (Life Technologies) with 2% FBS 2 days before transfection. The cells were transfected with 9 μg of control shRNA (pLKO.1) and shRNA against HIF-1α (shHIF-1α: lentiviral vector containing shRNA against HIF-1a) plasmids along with 6 μg of psPAX2 and 3 μg of pMD2.G. After 16 hours, the transfection medium was removed and replaced with DMEM with 10% heat-inactivated FBS and penicillin-streptomycin. Lentiviral particles were harvested at 48 hours and 60 hours posttransfection. NP cells were plated in DMEM with 10% heat-inactivated FBS 1 day before transduction. Cells in 10-cm plates were transduced with 5 mL of conditioned media containing viral particles along with 8 μg/mL hexadimethrine bromide

(commercial brand name Polybrene). After 24 hours, media was removed and replaced with DMEM with 10% FBS and continued for 3 days. The cells were cultured in hypoxia or normoxia for an additional 24 hours and harvested for protein and mRNA extraction 5 days after transduction.

Bioinformatics analysis

The nucleotide sequence and chromosomal location of the 2-kb proximal promoter of rat Car9 and Car12 were found using the UCSC Table Browser (UCSC Genome Informatics Group, Santa Cruz, CA, USA; https://genome.ucsc.edu/cgi-bin/hgTables). Evolutionary conservation of the 2-kb proximal promoter was determined using the Evolutionary Conserved Region (ECR) Browser (http://ecrbrowser.dcode.org/) with a threshold of 77%. Putative hypoxia-responsive element (HRE) consensus sequences (5′-[A/G]CGTG-3′) were determined using the JASPAR Core Database (http://jaspar.genereg.net/) with a relative score threshold of 0.85.[47] Multiz alignment of HRE motifs was performed using the Ensembl Lastz Database (European Bioinformatics Institute [EMBL-EBI]/Wellcome Trust Sanger Institute, Hinxton, UK; http://www.ensembl.org/index.html).

Chromatin immunoprecipitation

Rat NP cells were plated in 10-cm plates and either cultured in normoxia or hypoxia for 24 hours. Chromatin immunoprecipitation (ChIP) assay was performed using ChIP-IT high sensitivity kit (Active Motif, Carlsbad, CA, USA) according to the manufacturer's recommendations. Briefly, chromatin was sheared by sonication, and input DNA was generated by treating aliquots with RNase, proteinase K, and heat, followed by ethanol precipitation. DNA complexes were immunoprecipitated by incubation with anti-HIF-1α antibody (Cell Signaling) overnight at 4°C followed by binding to protein G-agarose beads for 3 hours at 4°C. Cross-links were reversed by treatment with proteinase K and heat for 2.5 hours, and DNA was purified using DNA purification elution buffer (Active Motif). Real-time PCR analysis was performed using ChIP-IT quantitative PCR analysis kit (Active Motif) using the following primer pairs for putative HRE sites (from JASPAR database[47]) as shown in Supplemental Table S1.

Negative control primers and standard curve primers used were provided with the ChIP-IT kit. Real-time PCR was performed with Power SYBR Green PCR Master Mix (Applied Biosystems). The threshold cycle (C_t) values were recorded, and the data were normalized based on primer efficiency, input DNA C_t values, amount of chromatin, and resuspension volume, based on the manufacturer's recommendations.

Cell viability assay

Rat NP cells were plated in a 96-well plate at 10,000 cells per well. Cells were incubated in hypoxia for 24 hours prior to treatment with three carbonic anhydrase inhibitors for 18 hours, 48 hours, and 96 hours. Viability was measured using Calcein-AM and Ethidium homodimer-1 dyes following standard protocol. Negative control (dead) cells were fixed with 70% methanol for 30 min at 37°C.

Mitochondrial oxidoreductase activity measurement

Rat NP cells were plated in a 96-well plate at 5000 cells per well. Cells were incubated in hypoxia for 24 hours prior to treatment with three carbonic anhydrase inhibitors for 18 hours. Oxidoreductase activity was measured using 3-(4,5-dimethylthiazol-2yl)-2,5-diphenyltetrazolium bromide (MTT) dye following standard protocol.

Extracellular lactate measurement

Rat NP cells were plated in duplicate in a six-well plate at 200,000 cells per well. Cells were incubated in hypoxia for 24 hours prior to treatment with three carbonic anhydrase inhibitors for 18 hours. Lactate concentrations were measured in each sample using a clinical lactate measurement kit from Trinity Biotech USA Inc. (Jamestown, NY, USA), complete with reagents and standard curve set.

pH_i measurement

Rat NP cells were plated in a 96-well plate at 10,000 cells per well. Cells were incubated in hypoxia for 24 hours prior to treatment with three carbonic anhydrase inhibitors for 18 hours. pH_i was measured following the pHrodo Red AM Intracellular pH Indicator (ThermoFisher) protocol. A standard curve was calculated by clamping the pH_i using extracellular buffers with a pH of 4.5, 5.5, 6.5, and 7.5 after treatment with a 10 μM valinomycin/nigericin ionophore cocktail.

Statistical analysis

All experiments were performed in triplicate at minimum, and data are presented as mean $\pm$ SE. Differences between groups were analyzed by the Student's *t* test and one-way ANOVA; $p < 0.05$.

Results

Hydration of CO_2, rather than glycolytic production of lactate, contributes more to the extracellular proton production in NP cells

In order to elucidate the baseline metabolism of NP cells we measured ECAR and OCR of primary NP cells with a Seahorse XF Analyzer after 24 hours of hypoxic culture (Fig. 1*A*, *B*). It was apparent from the ECAR and OCR time-courses that basal metabolic rates in NP cells were relatively low; especially OCR, which is 10-fold lower than those seen in other cell types.[48,49] Interestingly, inhibiting the electron transport chain with Antimycin A had no effect on ECAR or OCR, confirming that NP cells relied minimally on mitochondria for energy generation (Fig. 1*A*, *B*).[10]

Recently, Mookerjee and colleagues[24] elegantly showed that there are two major sources of extracellular production which contribute to ECAR measurements. Although ECAR measurements are generally used to solely report the glycolytic production of lactate/ H^+, CO_2 produced from the tricarboxylic acid (TCA) cycle can be enzymatically hydrated into HCO_3^- and H^+ units by membrane-associated and extracellularly-facing carbonic anhydrases (Fig. 1*C*). Although we have previously shown that that NP cells do not rely on mitochondria for ATP production, it is well known that the TCA cycle is necessary for generating the metabolic precursors for fatty acid, nucleotides, and amino acid synthesis.[10] With this understanding, we sought to determine the proportion of total proton production rate (PPR_{tot}) generated from glycolysis (PPR_{glyc}) and CO_2 hydration (PPR_{CO2}) according to the equations derived and modeled by Mookerjee and colleagues[24] (Fig. 1*D*):

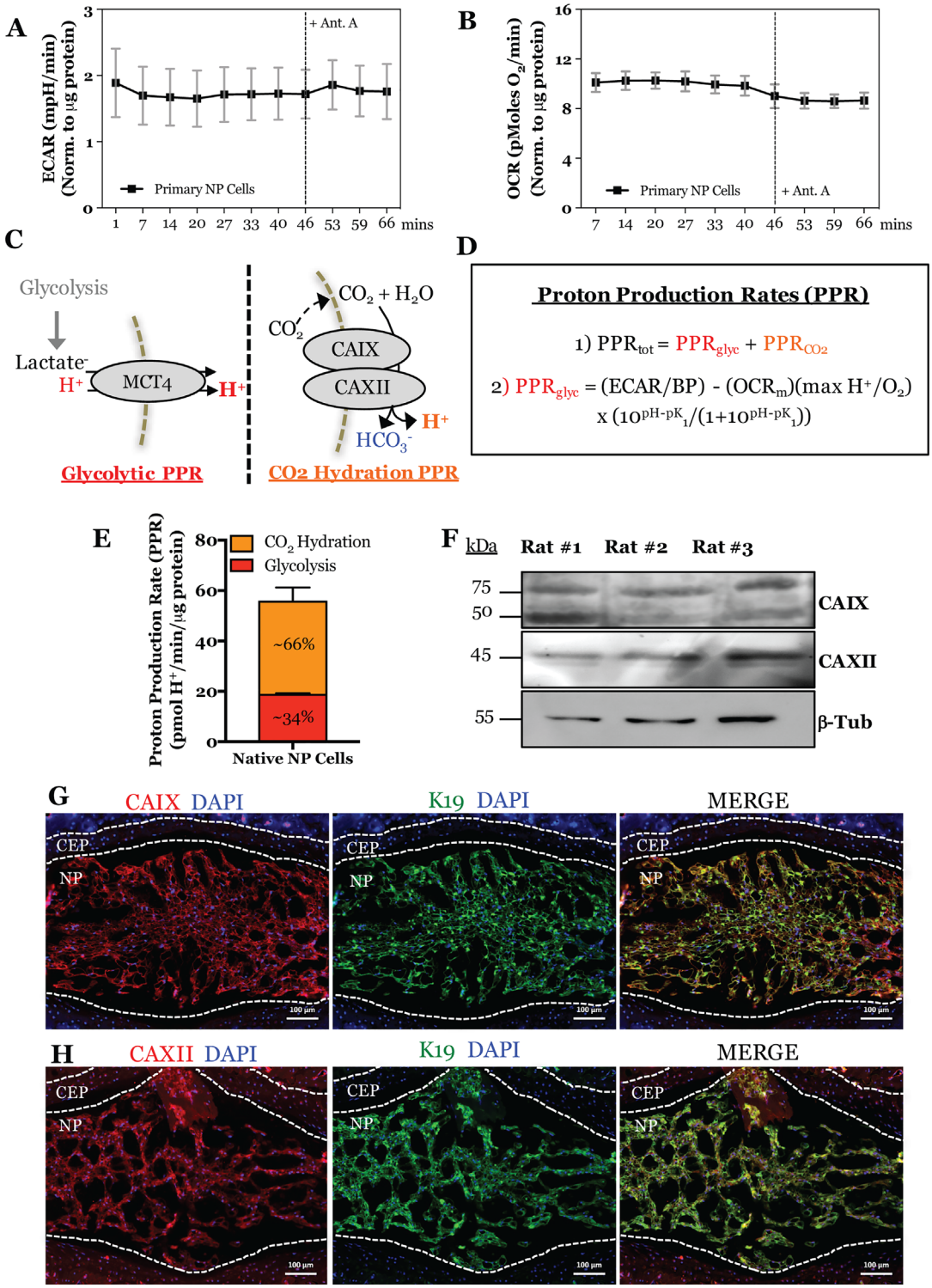

Fig. 1. Relative contribution of glycolysis and CO_2-hydration on rates of total extracellular proton production; expression of plasma-membrane associated extracellularly-facing CA isoforms in the intervertebral disc. (*A*) ECAR time-course showing proton production rate in primary NP cells before and after Antimycin A treatment. (*B*) OCR time-course showing total oxygen consumption in primary NP cells before and after Antimycin A treatment. (*C*) Schematic of two major cellular pathways contributing to extracellular proton production measured by the Seahorse XF Analyzer. (*D*) Equations derived from Mookerjee and colleagues[24] to determine the relative contribution of glycolysis and CO_2 hydration on total extracellular proton production rate. (*E*) Graphical representation of glycolytic and CO_2-derived proton production rates in the primary NP cells. (*F*) Representative Western blot analysis of CAIX and CAXII protein expression from NP tissue of 3 adult rats. (*G*, *H*) Immunofluorescence detection of CAIX (*G*), CAXII (*H*), and K19 (an NP cell marker) in the NP and CEP of tail discs. All quantitative data are represented as mean ± SE, $n = 3$ independent biological replicates with 4 technical replicates per biological replicate; 3 independent biological replicates were analyzed for immunofluorescence. Scale bar = 100 µm. CEP = cartilaginous endplate; PPR = proton production rate; BP = buffering power; β-Tub = β-tubulin; mpH = milli pH unit.

$$PPR_{tot} = PPR_{glyc} + PPR_{CO_2} \quad (1)$$

$$PPR_{glyc} = (ECAR/BP) - (OCR_m)(\max H^+/O_2) \times \left(10^{pH-pK_1}/\left(1 + 10^{pH-pK_1}\right)\right) \quad (2)$$

where PPR_{CO_2} = proton production rate derived from extracellular CO_2 hydration, BP = buffering power (mpH/pmol H^+), OCR_m = mitochondrial oxygen consumption rate (pmol O_2/min), pH = pH of the assay conditions, and pK_1 = equilibrium constant of CO_2 hydration: $CO_2(aq) + H_2O \rightarrow HCO_3^- + H^+ = 6.093$ at 37 °C.

We determined the glycolytic proton production rate in primary NP cells (using glucose and glutamine as substrates) to be 18.8 to 19.2 pmol H^+/min/μg protein. Given that the total proton production rate of 56 ± 5 pmol H^+/min/μg protein, the percentage of total proton production generated from glycolysis is 34% ± 3% and from CO_2 hydration is 66% ± 3% (Fig. 1*E*). These results suggested that CO_2 hydration by extracellularly-facing carbonic anhydrases should be critical in NP cell physiology.

Carbonic anhydrase isoforms 9 and 12 are expressed in intervertebral disc tissue in vivo

In order to confirm the presence of carbonic anhydrases 9 and 12 in intervertebral disc tissue, we isolated total protein from the NP tissue of adult rats. Western blot analysis confirmed the robust expression of both CAIX and CAXII protein in the native NP tissue (Fig. 1*F*). Furthermore, intervertebral disc sections were immunolabeled with antibodies against CAIX and CAXII, and cytoskeletal Keratin-19 (K19), a known NP phenotypic marker, to elucidate their tissue localization in vivo.[45] CAIX (Fig. 1*G*) and CAXII (Fig. 1*H*) were predominantly located in the NP with lower level expression in the AF and endplates (Supplemental Fig. S1). Furthermore, most cells in the NP compartment were visibly immunopositive for CAIX and CAXII antibody staining, respectively, implying that both isoforms are co-expressed (Supplemental Fig. S1). These results suggested that the expression of these two CA isoforms is enriched in the NP compartment of the adult intervertebral disc and may play an important role in tissue physiology.

Expression of carbonic anhydrase isoforms is hypoxia-inducible in NP cells

Given the robust expression of CA9 and CA12 in the NP tissue, we investigated the effect of oxygen tension on their mRNA and protein levels. We cultured primary rat NP cells under hypoxic conditions for 8 to 72 hours and measured mRNA and protein expression by qRT-PCR and Western blot. Car9 and Car12 mRNA showed significant hypoxic induction as early as 8 hours and persisted until 72 hours (Fig. 2*A*, *B*). Among both CA isoforms, the magnitude of induction was highest for Car12; levels were ~15-fold after 8 hours and remained elevated (~10-fold) at 72 hours in hypoxia (Fig. 1*B*). Additionally, an Actinomycin D chase assay showed that Car9 and Car12 mRNA had enhanced stability under hypoxia. The half-life ($t_{1/2}$) of Car9 mRNA increased from 13.6 to 19.7 hours in hypoxia. Likewise, the half-life of Car12 mRNA increased from 11.5 to 16.8 hours (Fig. 2*C*, *D*). These results imply that Car9 and Car12 mRNA is stabilized by posttranscriptional regulation under hypoxia. Likewise, CAIX (Fig. 2*E*, *F*), and CAXII protein (Fig. 2*E*, *G*) levels were also elevated after 72 and 24 hours in hypoxia, respectively. Overall, it is evident that CA9 and CA12 are sensitive to changes in oxygen tension and their expression was upregulated under hypoxic conditions. Moreover, we show here for the first time that CA9, in addition to CA12, is hypoxia sensitive in NP cells.[42]

HIF-1α binds to select HRE binding regions in the promoters of Car9 and Car12 in hypoxic NP cells

HIF-1α binds HREs in the gene promoters of downstream targets for transactivation. The precise locations of HRE consensus sequence (5′-[A/G]CGTG-3′) within rat Car9 and Car12 promoters were predicted using a transcription factor binding databases JASPAR CORE database.[47] Analysis identified several putative HRE binding sites on the promoters of Car9 and Car12 (Fig. 2*H*). Next, the sequence conservation of the putative HRE motifs was analyzed using Multiz alignment tool from the Ensembl Lastz database (http://www.ensembl.org/index.html), which showed 100% conservation at HRE R1 in Car9 and HRE R1 and R3 in Car12 promoters (Fig. 2*I*). We experimentally validated HIF-1α binding to these predicted HRE regions on Car9 and Car12 promoters in rat NP cells using genomic ChIP. Of the three putative HRE binding regions on the Car9 promoter, the region with the highest conservation and closest to the transcriptional start site showed binding independent of oxemic tension (Fig. 2*J*). This result was not unexpected for NP cells, which constitutively express HIF-1α even under normoxic conditions.[4,5] Interestingly, of three putative HRE binding regions on the Car12 promoter, binding was seen only at HRE R1, which also showed enrichment in hypoxia (Fig. 2*K*).

CA9 and CA12 expression is regulated by HIF-1α in NP cells in vitro

We have previously shown[10] the importance of HIF-1α for maintaining NP cell function and phenotype within the hypoxic niche of the intervertebral disc. Unique to NP, HIF-1α shows stabilized expression even under normoxic conditions.[4,5] Because expression of CA isoforms in NP cells is hypoxia sensitive and HRE regions in the Car9 and Car12 promoters bind HIF-1α, we sought to delineate their relationship using HIF-1α gain and loss of function approaches. Stabilizing HIF-1α protein with DMOG treatment for 8 hours showed a small increase in Car9 mRNA levels, induction was lost at 24 hours (Fig. 3*A*), whereas Car12 mRNA levels were significantly increased (Fig. 3*B*). Importantly, we also transduced rat NP cells with lentiviruses expressing two HIF-1α shRNA sequences. This silencing approach resulted in a stable ~90% knockdown of HIF-1α (Fig. 3*C*, *F*, *G*). CA9 mRNA and protein expression was significantly reduced by HIF-1α silencing under both normoxia and hypoxia (Fig. 3*D*, *F*, *H*). Likewise, HIF-1α silencing resulted in a significant decrease in CA12 mRNA and protein expression in hypoxia (Fig. 3*E*, *F*, *I*). Taken together, our loss of function studies implied that expression of CA9 and CA12 is regulated by HIF-1α in NP cells.

CA9 and CA12 expression is reduced in the discs of NP-specific HIF-1α knockout mice

Our in vitro results clearly suggest that CA9 and CA12 expression is HIF-1α–dependent in NP cells. To further support this observation, we investigated the effect of HIF-1α deletion on CA9 and CA12 expression in vivo using an NP-specific HIF-1α knockout mouse, where HIF-1α deletion was achieved by constitutive Cre expression driven by a notochord-specific Foxa2

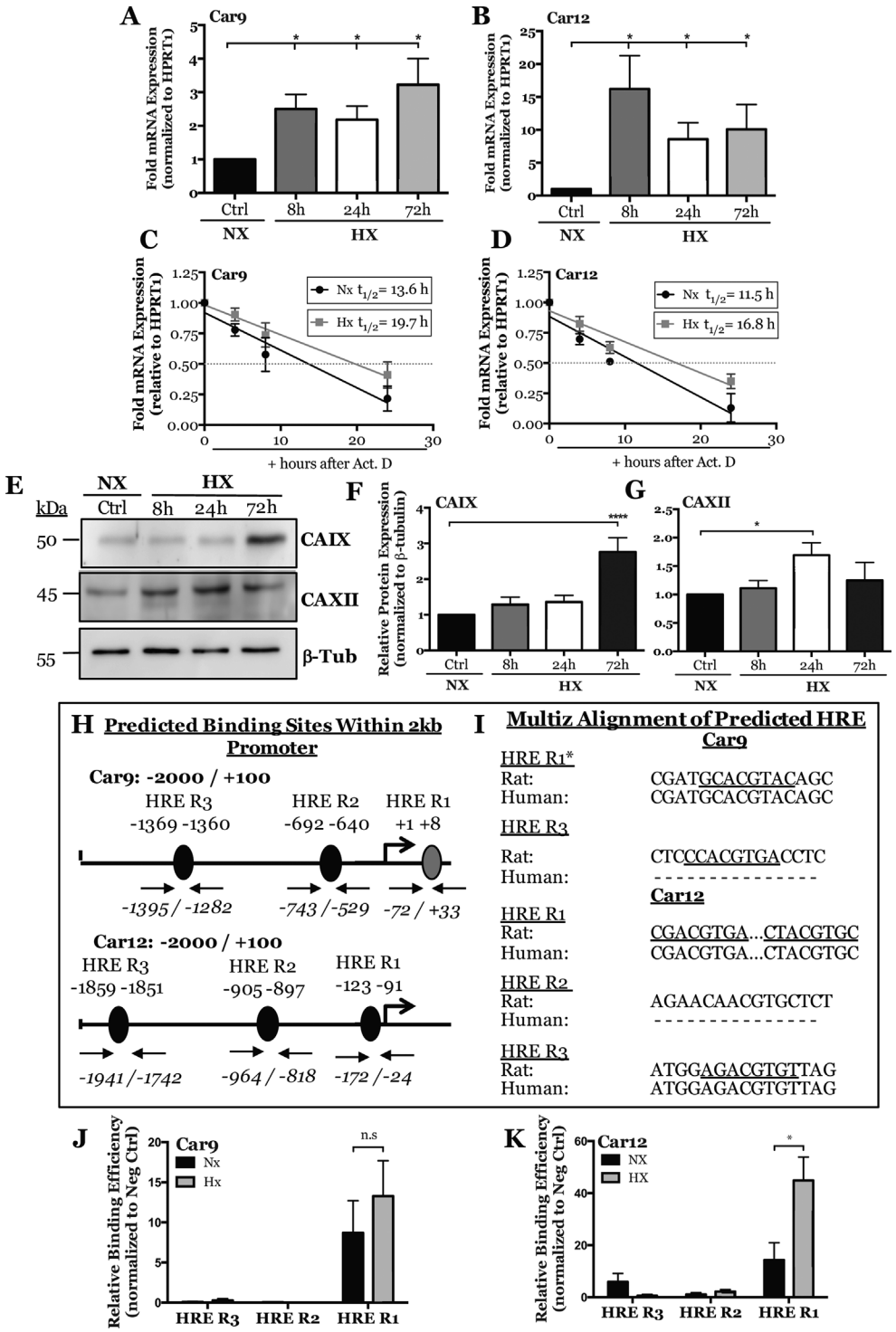

Fig. 2. Effect of hypoxia on CA9 and CA12 expression, bioinformatic analysis of HRE motifs in Car9 and Car12 promoters, and ChIP analysis. (*A*, *B*) qRT-PCR analysis of Car9 (*A*), and Car12 (*B*) mRNA expression in rat NP cells cultured under hypoxia (1% O_2) for up to 72 hours. (*C*, *D*) Actinomycin D chase assay showing regression curve of Car9 (*B*) and Car12 (*C*) mRNA at 0, 4, 8, and 24 hours after Actinomycin D treatment (5 μg/mL). An increase in mRNA half-life ($t_{1/2}$) is seen for both genes in hypoxia. (*E*) Western blot analysis of CAIX and CAXII protein expression in rat NP cells cultured under hypoxia for up to 72 hours. (*F*, *G*) Densitometric analysis of CAIX (*F*) and CAXII (*G*) from Western blot experiment shown in *E*. (*H*) JASPAR predicted HRE regions (5′-[A/G]CGTG-3′) within −2000/+100 bp into the rat *Car9* and *Car12* promoters with a relative score threshold of 0.85. Predicted HRE regions (black); conserved binding regions validated in human promoter (gray). (*I*) Multiz alignment from Ensembl Lastz database. Core matrix binding locations are underlined, inability to match shown by (-), * sequences are from the negative strand. (*J*, *K*) Relative binding efficiency of HIF-1α to putative HRE regions in the rat Car9 (*J*) and Car12 (*K*) promoters determined by ChIP. Statistical analysis performed on HRE regions with ≥5 HIF-1α binding events/1000 cells and binding efficiency fivefold greater than negative control. Data are represented as mean ± SE, $n \geq 3$ biological replicates, $p < 0.05$. β-Tub = β-tubulin; HX = hypoxia; NX = normoxia.

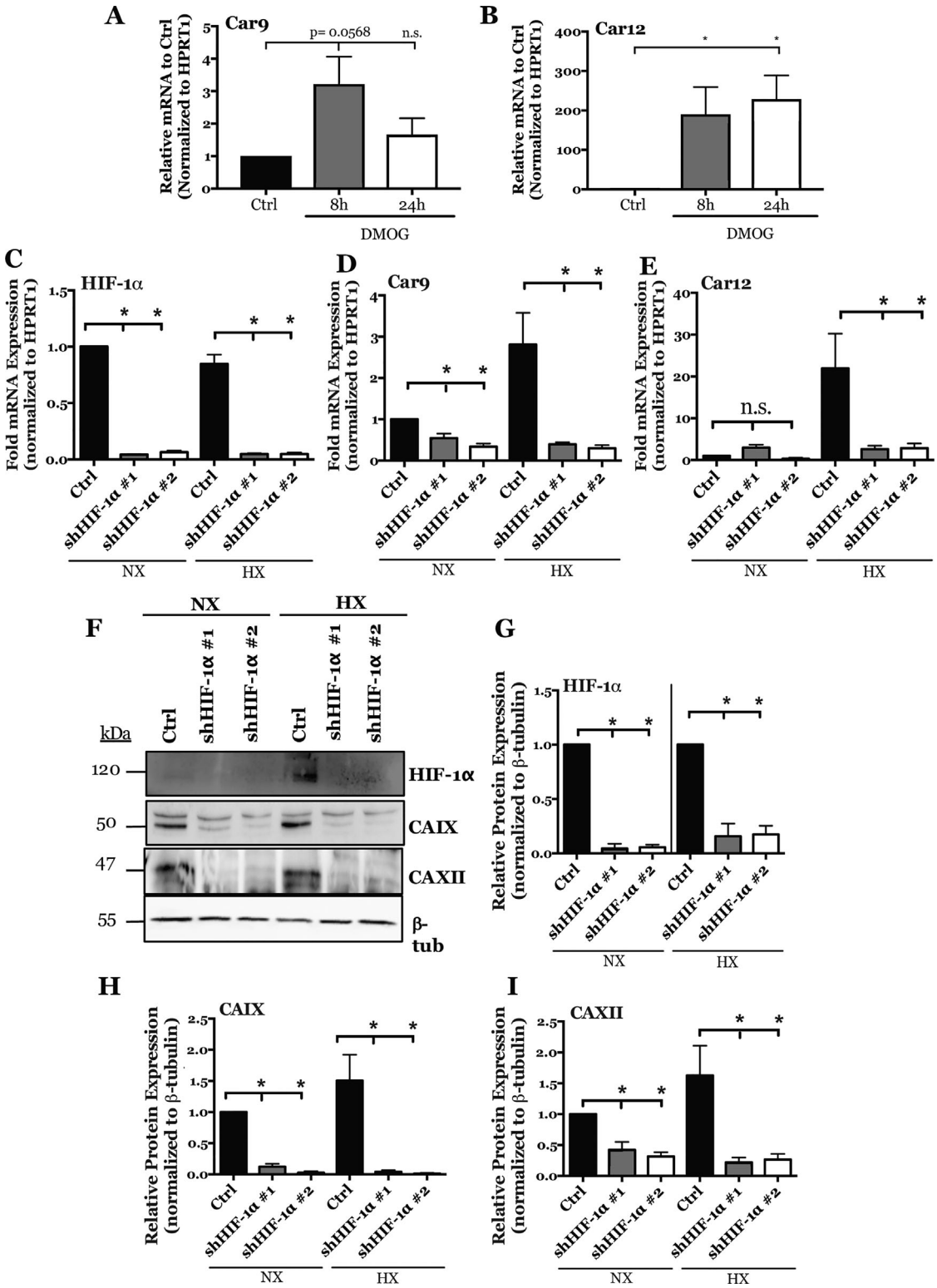

Fig. 3. HIF-1α gain and loss of function in NP cells effects CA9 and CA12 expression. (*A*, *B*) Effect of stabilizing HIF-1α protein with DMOG treatment for 8 and 24 hours on Car9 (*A*) and Car12 (*B*) expression. (*C–E*) qRT-PCR analysis of HIF-1α (*C*), Car9 (*D*), and Car12 (*E*) mRNA expression in rat NP cells after silencing HIF-1α with two lentiviruses, each expressing an independent HIF-1α targeting shRNA (shHIF-1α #1 and shHIF-1α #2). (*F*) Representative Western blot analysis of HIF-1α, CAIX, and CAXII protein expression in rat NP cells after silencing HIF-1α with two independent shRNAs. (*G–I*) Densitometric analysis of Western blot shown in *F*. Data are represented as mean ± SE, $n \geq 4$ independent biological replicates, $p < 0.05$. β-Tub = β-tubulin; HX = hypoxia; NX = normoxia.

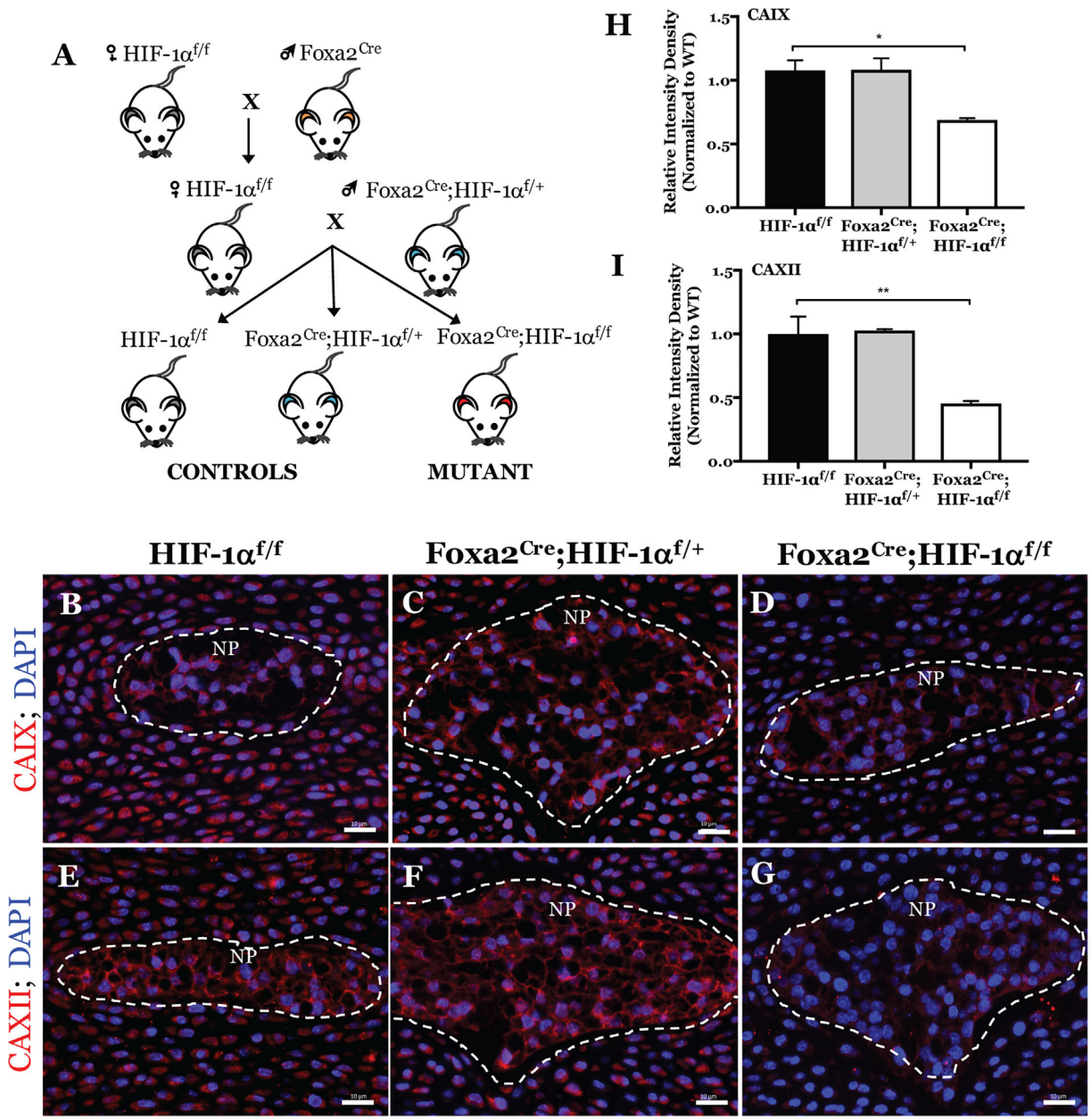

Fig. 4. Mice with NP-specific deletion of HIF-1α show decreased expression of CAIX and CAXII in NP tissue. (*A*) Schematic breeding diagram for generation of NP-specific HIF-1α knockout mice (Foxa2^{Cre};HIF-1α$^{f/f}$) from heterozygous Foxa2^{Cre} and control HIF-1α$^{f/f}$ mice. (*B–G*) Representative immunofluorescence images of CAIX (*B–D*) and CAXII (*E–G*) expression in E15.5 control (*B*, *E*: HIF-1α$^{f/f}$), heterozygous (*C*, *F*: Foxa2^{Cre}; HIF-1α$^{f/+}$), and HIF-1α mutant (*D*, *G*: Foxa2^{Cre};HIF-1α$^{f/f}$) littermate mice imaged at magnification ×20. NP compartment denoted by white dashed line. (*H*, *I*) Quantification of CAIX (*H*) and CAXII (*I*) staining intensity density (integrated density per NP tissue area) in control and HIF-1α cKO mice. Three conditional null and littermate controls were analyzed. Scale bar = 20 μm. cKO = conditional knockout.

promoter/enhancer (Fig. 4*A*).[46] We chose to analyze CA expression at E15.5 because, at this stage the NP is completely formed and, in null mice, NP cells undergo apoptosis at birth.[46] We labeled disc sections of E15.5 HIF-1α mutant mice (Foxa2^{Cre}; HIF-1α$^{f/f}$) and control littermates with antibodies against CAIX and CAXII, and analyzed expression with fluorescent microscopy (Fig. 4*B–G*). We observed that the expression of both CAIX (Fig. 4*B–D*) and CAXII (Fig. 4*E–G*) was reduced in the NP (indicated by the white dotted line) of HIF-1α mutant mice (Fig. 4*D*, *G*) compared to heterozygous (Foxa2^{Cre};HIF-1α$^{f/+}$) (Fig. 4*C*, *F*) and wild-type (HIF-1α$^{f/f}$) (Fig. 4*B*, *E*) littermate controls. A significant decrease in CAIX (Fig. 4*H*) and CAXII (Fig. 4*I*) staining intensity was confirmed in the HIF-1α mutant mice by measuring integrated staining density per NP area.

These results confirm the role of HIF-1α in maintaining levels of CAIX and CAXII in NP tissue.

Inhibition of CAs reduces ECAR and total OCR in NP cells without affecting mitochondrial OCR

The precise contribution of carbonic anhydrases in NP cell physiology is still unknown. To elucidate the role of CA9 and CA12 in NP cell metabolism and acid-base homeostasis we measured changes in ECAR and OCR with a Seahorse Analyzer following treatment of NP cells with specific CA inhibitors in hypoxia for 18 hours. Although MZA and AZA are pan-carbonic anhydrase inhibitors, at the concentrations used in this study, they specifically inhibited CA9 and CA12 catalytic function in NP cells,[50] whereas U-104 is a specific inhibitor of CA9 and CA12 ($K_i = 45$ nM and 4.5 nM, respectively) with very low inhibition for CA1 and CA2 ($K_i = 5080$nM and 9640nM, respectively).[43] When this inhibitor is used, the cytosolic CA isoforms expressed in the disc (CA2/3) will not be affected, given the high K_i for CA2 and known inability of CA3 to be effectively inhibited with small molecules.[51] First, we confirmed that changes in cell viability did not confound metabolic profiling; inhibition of CA function for 18 hours did not significantly affect cell viability (Fig. 5*A*). However, cells treated with MZA, AZA, and U-104 experienced significant decreases in ECAR over time (Fig. 5*B–D*) and on average (Fig. 5*E*); treatment with Antimycin A had no effect on ECAR, again suggesting minimal dependency on electron transport chain in NP cells (Fig. 5*B–E*). Overall, these results

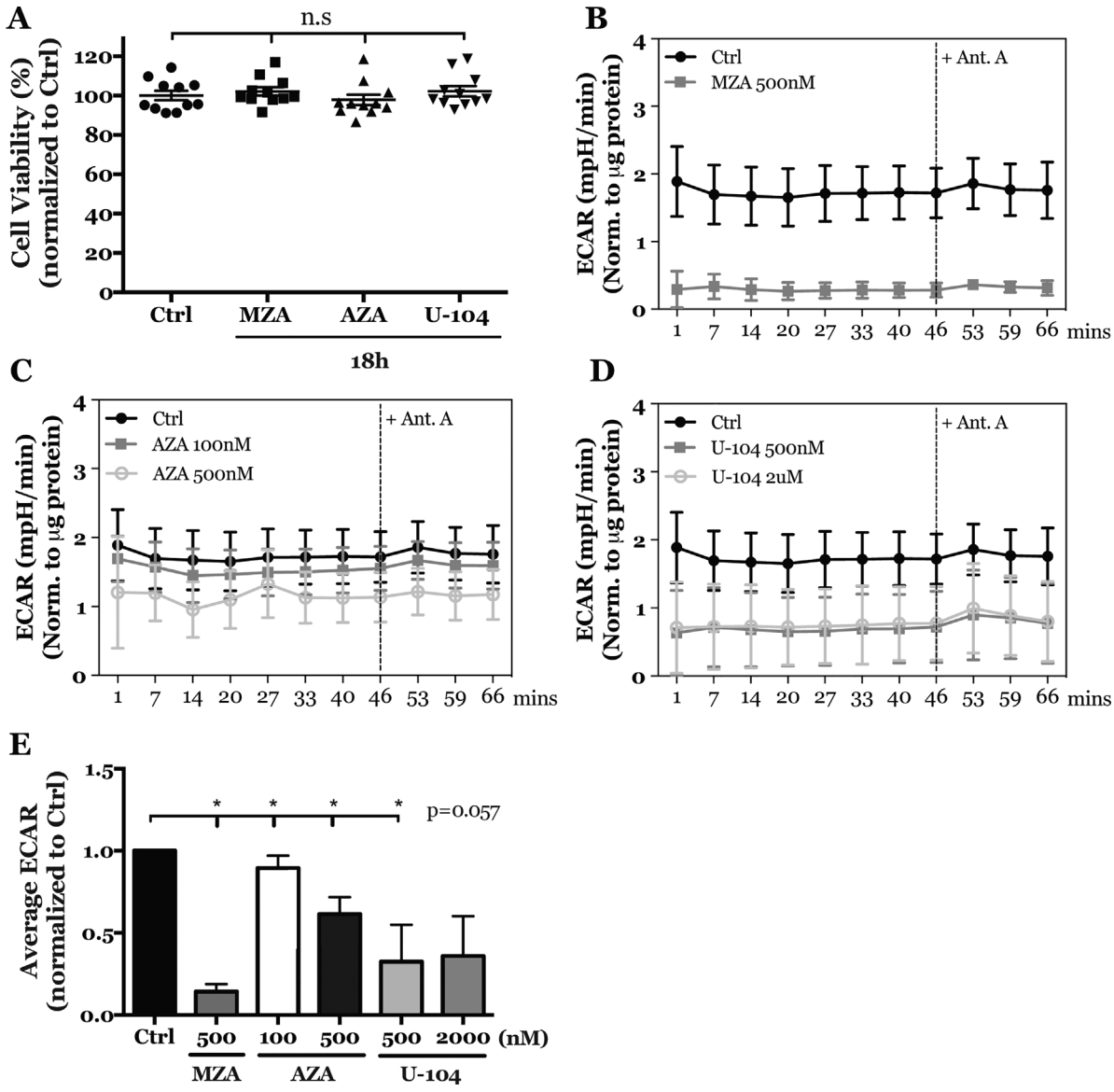

Fig. 5. Inhibition of CA9 and CA12 in rat NP cells leads to reduced ECAR. (*A*) Treatment of rat NP cells with MZA (500 nM), AZA (500 nM), and U-104 (2 μM) for 18 hours has no effect on cell viability. (*B–D*) ECAR was reduced in rat NP cells treated with MZA (500 nM) (*B*), AZA (100 nM, 500 nM) (*C*), and U-104 (500 nM, 2 μM) (*D*) before and after treatment with Antimycin A. (*E*) Average ECAR was significantly decreased before addition of Antimycin A. All quantitative data are represented as mean ± SE, $n = 3$ independent biological replicates with 4 technical replicates per biological replicate, $p < 0.05$. mpH = milli pH unit.

show that catalytic inhibition of CA9/12 decreased total extracellular proton production, confirming that extracellular acidification in NP cells is partially due to CA9/12-dependent hydration of CO_2.

Likewise, treatment with MZA, AZA, and U-104 significantly decreased total OCR over time (Fig. 6*A*–*C*) and on average (Fig. 6*D*). Notably, however, treatment with Antimycin A had no effect on OCR (Fig. 6*A*–*C*), suggesting that mitochondrial OCR was unaffected by CA inhibition (Fig. 6*E*). In addition, we confirmed that mitochondrial function was not altered with CA inhibition by measuring mitochondrial oxidoreductase activity (Fig. 6*F*). In summary, inhibition of CA catalytic activity decreased extracellular H^+ accumulation and oxygen consumption rates of NP cells, independent of mitochondrial oxidative respiration.

Inhibition of CAs causes a significant decrease to the total extracellular proton production rate without affecting glycolysis in NP cells

To investigate the functional effect of CA inhibition on NP cells we delineated the source of extracellular proton production that contributed to decreased ECAR; ie, H^+ produced via glycolysis or

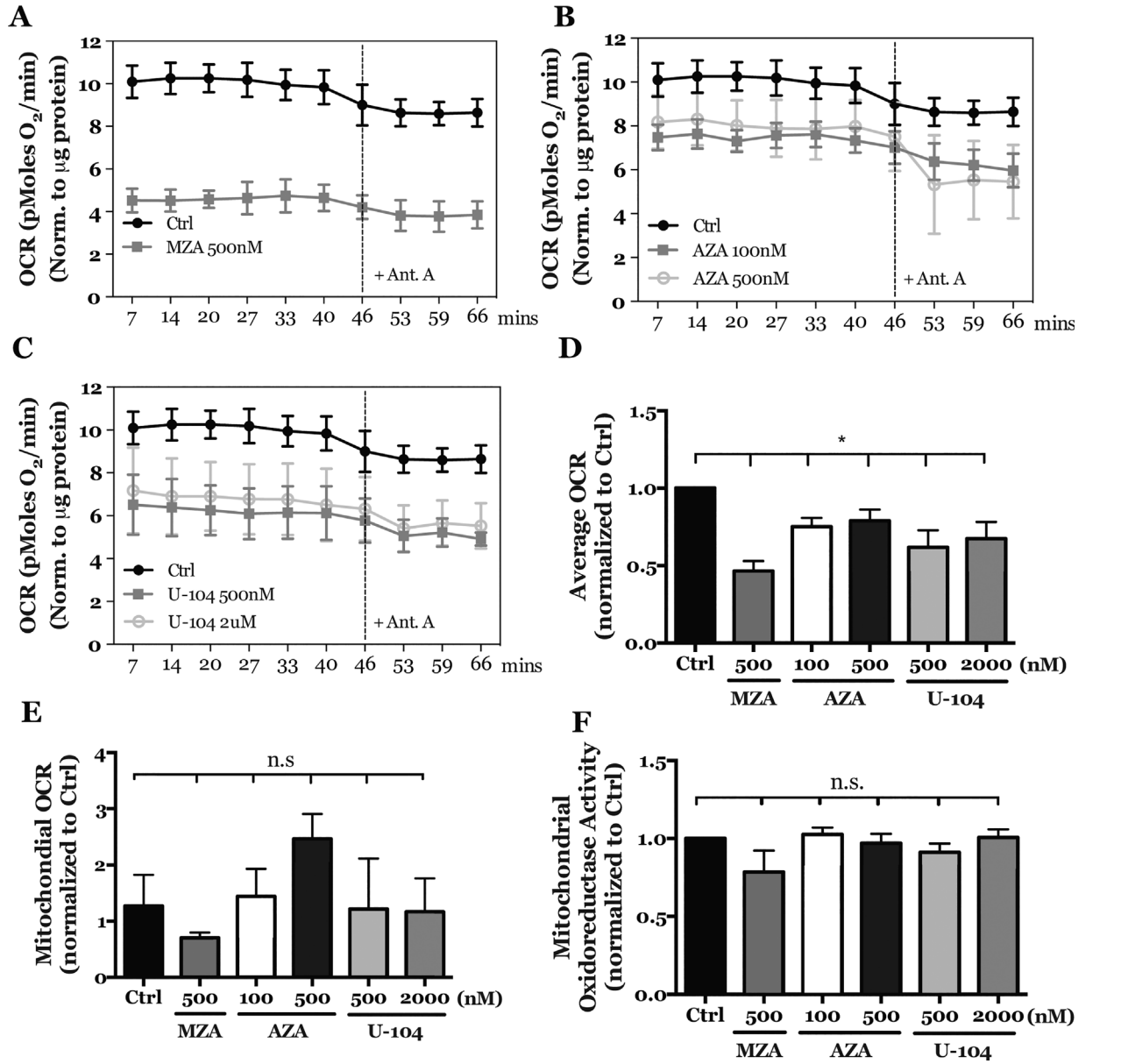

Fig. 6. Inhibition of CA9 and CA12 in rat NP cells leads to reduced OCR without affecting mitochondrial respiration or functional activity. (*A*–*C*) OCR was reduced in rat NP cells treated with MZA (500 nM) (*A*), AZA (100 nM, 500 nM) (*B*), and U-104 (500 nM, 2 µM) (*C*) before and after treatment with Antimycin A. (*D*) Treatment of rat NP cells with MZA, AZA, and U-104 significantly decreased average OCR. (*E*) Treatment of rat NP cells with MZA, AZA, and U-104 has no effect on mitochondrial OCR. (*F*) Rat NP cells treated with MZA, AZA, and U-104 showed no change in their mitochondrial oxidoreductase activity, implying preservation of mitochondrial function. All quantitative data are represented as mean ± SE, $n = 3$ independent biological replicates with 4 technical replicates per biological replicate, $p < 0.05$.

CO_2 hydration. Because we determined that ~66% of total proton production in NP cells is from extracellular CO_2 hydration, it is expected that part of the decrease in ECAR after CA inhibition is directly due to abrogating proton production from the CA reaction. However, the other potential source of extracellular proton production measured by the analyzer is those transported out of the cells with lactate via monocarboxylate transporter 4 (MCT4). This measurement is often considered a surrogate measure of glycolytic flux as MCT4 exports equal units of lactate and H^+, the end products of anaerobic glycolysis (Fig. 7*A*).[52]

To investigate if glycolytic flux was perturbed, we measured the effect of CA inhibition on HIF-1α, a major regulator of glycolysis. We showed that levels of HIF-1α protein (Fig. 7*B*, *C*)

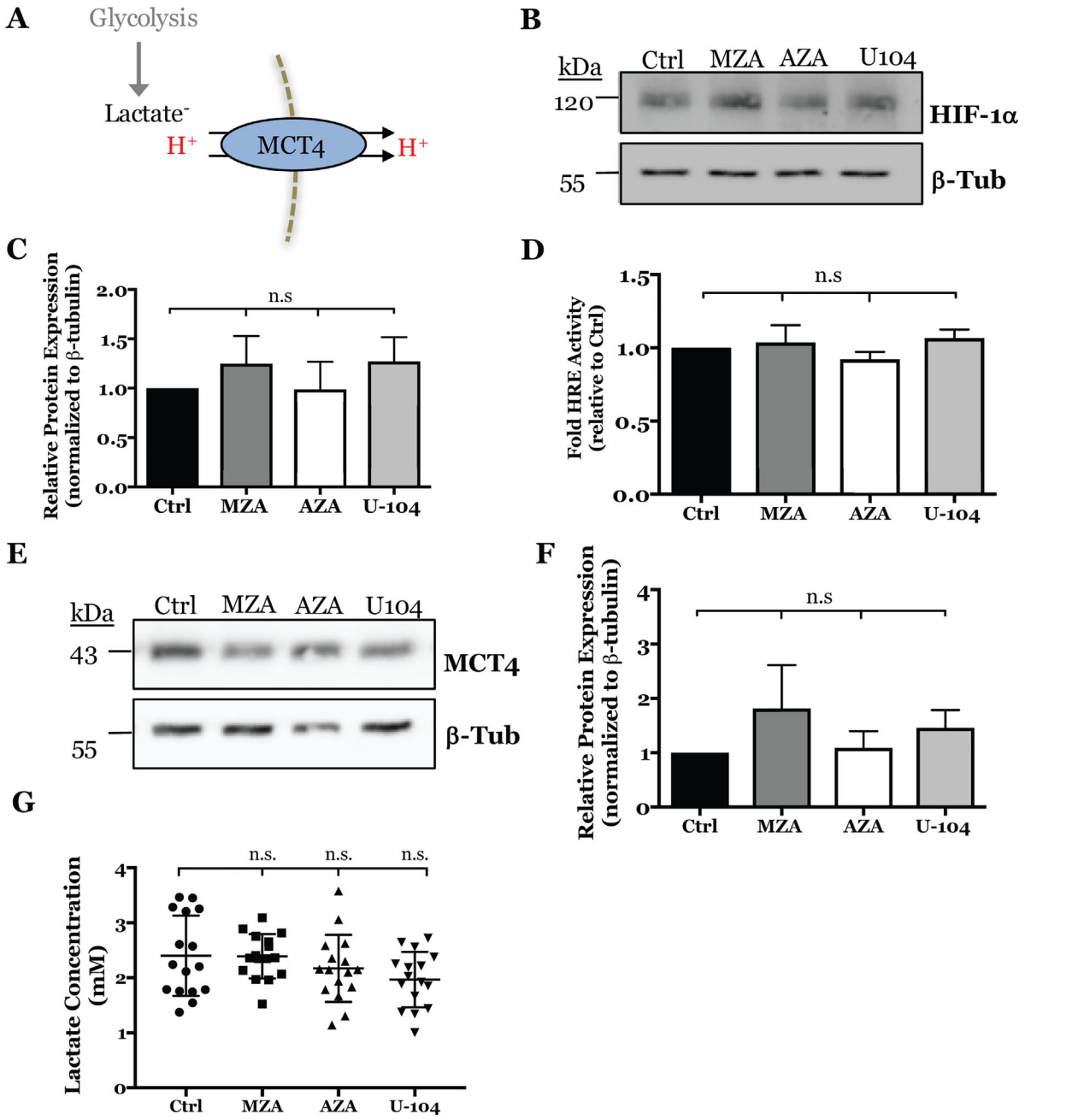

Fig. 7. Inhibition of CA9 and CA12 in rat NP cells has no effect on glycolytic flux. (*A*) Schematic of the glycolytic production of lactate/H^+ exported into the extracellular space via MCT4. (*B*) Representative Western blot analysis of HIF-1α after inhibiting CA activity with MZA (500 nM), AZA (500 nM), and U-104 (2 μM) for 18 hours in hypoxia. (*C*) Densitometric analysis of Western blot experiment shown in *B* ($n = 4$). (*D*) HRE luciferase reporter activity was unaffected by CA inhibition ($n = 4$; 3 technical replicates each). (*E*) Representative Western blot analysis of MCT4 after inhibiting CA activity with MZA, AZA, and U-104. (*F*) Densitometric analysis of Western blot experiment shown in *E* ($n = 4$). (*G*) Extracellular lactate concentrations were unaffected by CA inhibition with MZA, AZA, and U-104 ($n = 5$; 3 technical replicates each). Data are represented as mean ± SE, $n \geq 4$ independent biological replicates, $^{*}p < 0.05$, $^{**}p < 0.01$, $^{***}p < 0.001$. β-Tub = β-tubulin.

and HIF-1α transcriptional activity measured by HRE luciferase reporter is unaltered (Fig. 7*D*). We also confirmed that MCT4 protein levels did not change after inhibiting CAs (Fig. 7*E*, *F*) and that extracellular lactate concentrations remained unaffected by CA inhibitors (Fig. 7*G*). Taken together, these results suggested that the decrease in extracellular proton production contributing to decreased ECAR was not due to a change in glycolytic flux or lactate transport. Rather, the data confirm that catalytic activity of extracellularly facing CAs favors the hydration of CO_2 generating H^+ and HCO_3^- ions, and inhibition of this reaction causes a measurable decrease in extracellular H^+ and HCO_3^- units.

Unlike CA inhibition, silencing of HIF-1α causes a shift from glycolytic to oxidative metabolism in NP cells

Because our results clearly showed that CA9 and CA12 are HIF-1α targets, we determined if the metabolic profile of NP cells following CA inhibition is like that of cells lacking HIF-1α. Similar to effect of CA inhibition on ECAR, HIF-1α silencing significantly decreased ECAR compared to cells transduced with shCtrl (scrambled lentiviral vector for expression of shRNA; control shRNA plasmid); importantly however, this reduction was rescued by blocking mitochondrial function with Antimycin A (Fig. 8*A*, *B*). These results suggest that the reduction in ECAR by HIF-1α silencing is likely caused by a rewiring of substrate flux, such that pyruvate is now diverted into the mitochondria and away from reduction to lactate. Moreover, the subsequent increase in ECAR upon antimycin treatment indicated that the HIF-1α–silenced cells retain reserved glycolytic capacity.

HIF-1α silencing also caused a significant increase in total OCR (mitochondrial + non-mitochondrial). Interestingly, this increase was substantially suppressed by Antimycin A (Fig. 8*C*). We determined the mitochondrial fraction of total OCR and found that HIF-1α silencing increased not only the total OCR but also the mitochondrial OCR fraction (Fig. 8*D*, *E*). Furthermore, we calculated rates of glycolytic and CO_2-dependent proton production and found that HIF-1α knockdown decreased the relative contribution from glycolysis and increased the contribution from CO_2 hydration (total proton production rate was ~65 and ~55 pmol H^+/min/μg protein for the shCtrl and shHIF-1α group, respectively), suggesting an increase in TCA-cycle derived CO_2 (Fig. 8*F*). Given that the results of HIF-1α knockdown assays implied that NP cells are capable of oxidative metabolism, we determined whether NP cells possess reserve electron transport chain capacity by uncoupling mitochondrial ATP generation from electron transport chain activity using the chemical uncoupler, FCCP (Fig. 8*G*). Interestingly, the fold change in OCR increased in a dose-dependent manner with FCCP treatment from 400 to 1000 nM concentrations. These data suggest that NP cells do, in fact, have reserve electron transport chain capacity that can be tapped into under specific circumstances, such as when HIF-1 signaling is compromised. Taken together, these results clearly showed that HIF-1α actively suppresses electron transport chain function and oxidative respiration in NP cells, and silencing this crucial transcription factor caused a shift in cellular metabolism beyond that evidenced by dysregulation of CAs.

Inhibition of CAs causes a significant decrease in pH_i by blocking the generation of recycled bicarbonate

Given that CA inhibition caused a significant decrease in extracellular H^+ and HCO_3^- production, we investigated the fate of this extracellular HCO_3^-. In some hypoxic cancer cells CA9/12-produced extracellular HCO_3^- is retrieved to buffer cytosolic pH[19,53] (Fig. 9*A*). We measured pH_i of rat NP cells after CA inhibition using fluorescent pH-sensitive probes. In line with previous studies of bovine NP cells, the baseline pH_i in rat NP cells was found to be acidic (pH ~6.8).[11] Importantly, our results clearly showed that the pH_i became more acidic when CA9/12 were inhibited (Fig. 9*B*). These results confirmed that the CA9/12 reaction indeed favors production of extracellular HCO_3^-, which is recycled to buffer pH_i. Noteworthy, we performed these experiments in HCO_3^- buffered medium to verify that the equilibrium of the CA reaction was not shifted to favor H^+ and HCO_3^- production as a reflection of the non-HCO_3^- buffered conditions in the Seahorse assay.

HCO_3^- recycling is dependent on the expression and function of bicarbonate transporters in the NP. Analysis of our previous RNA-Seq studies indicated that NP cells express various plasma membrane bicarbonate transporters of the SLC4 and SLC26 families (GEO Accession #GSE86552).[25] Of the bicarbonate transporters expressed, SLC4A2 (AE2), SLC4A4 (NBCe1), SLC4A7 (NBCn1), and SLC26A4 (Pendrin) had the highest levels. qRT-PCR results confirmed the expression of these four isoforms in rat NP cells (Fig. 9*C*). Na^+-coupled/HCO_3^- exchangers, NBCn1 and NBCe1, are known to function as HCO_3^- importers and can be catalytically inhibited by the Stilbene derivative, SITS.[35] We measured pH_i after inhibiting bicarbonate transport with SITS. The results recapitulated the significant decrease in pH_i seen after CA9/12 inhibition (Fig. 9*D*). This result indicated that HCO_3^- produced pericellularly by CA9 and CA12 activity is recycled by NP cells to buffer cytosolic pH.

Chronic inhibition of CA9 and CA12 in hypoxia results in NP cell death

Although short-term inhibition of CA9 and CA12 had no measurable effect on cell viability, we hypothesized that longer-term inhibition and resultant intracellular acidification will lead to pathological changes in NP cell viability. To test this, we measured NP cell viability after inhibiting CA9 and CA12 for 48 and 96 hours. Our results clearly demonstrate that NP cell viability decreased by 15% and 20% after 48 and 96 hours of CA inhibition, respectively (Fig. 9*E*).

Discussion

The avascular NP tissue relies on a predominantly glycolytic metabolism for energy generation.[10] Pathologically acidic pH (~6.5) exacerbates the breakdown of extracellular matrix proteins and decreases cellular glycolytic flux by NP cells[7,14–16]; as a result, cells tightly control metabolite concentrations to maintain a physiological pH_i. Carbonic anhydrases are the major regulators of acid-base metabolism in other cell types.[22] Despite their critical contribution in buffering intracellular and extracellular pH, the detailed molecular mechanisms that control expression of carbonic anhydrases and their function in hypoxic NP cells is not yet fully elucidated.[41,42] In this study, we showed for the first time that CO_2 hydration contributes to the majority of extracellular H^+ and HCO_3^- production in the NP cell matrix through actions of HIF-1–dependent membrane-associated and extracellularly facing carbonic anhydrase isoforms 9 and 12. Notably, our data support the contribution of CA9 and 12 to a HCO_3^- transport metabolon and pH_i regulation, underscoring their importance in NP physiology (Fig. 9*F*).

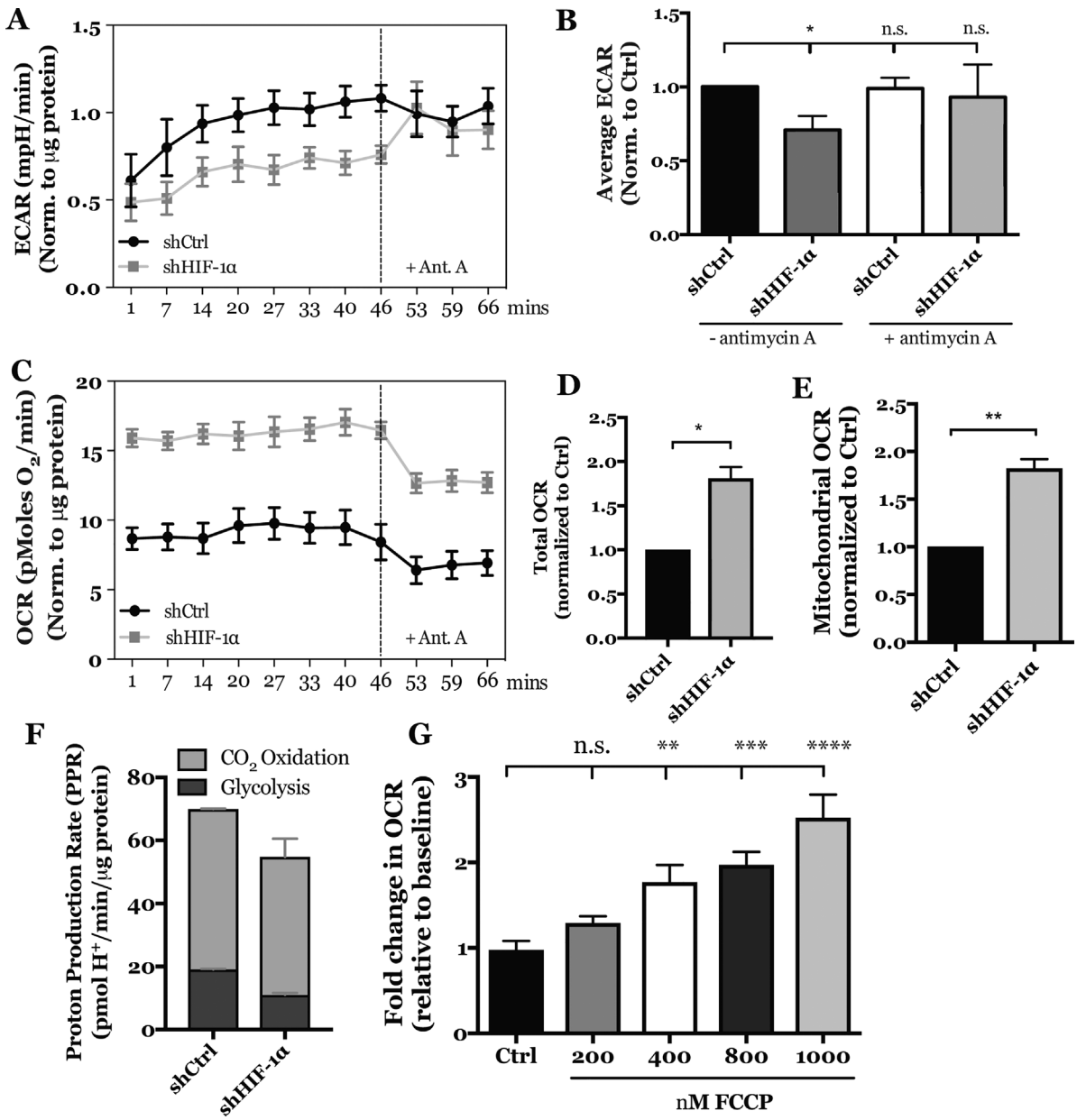

Fig. 8. HIF-1α silencing in rat NP cells leads to metabolic switch from glycolytic to oxidative metabolism. (*A*) Effect of stable HIF-1α silencing on ECAR of rat NP cells over time, before and after treatment with Antimycin A. (*B*) Stable HIF-1α knockdown led to decreased average ECAR compared to cells transduced with shCtrl, and treatment with Antimycin A rescued ECAR in HIF-1α–silenced cells. (*C*) Effect of stable HIF-1α silencing on OCR of rat NP cells over time, before and after treatment with Antimycin A. (*D*) Stable HIF-1α knockdown significantly increased total OCR (mitochondrial + non-mitochondrial) compared to cells transduced with shCtrl. (*E*) Stable HIF-1α knockdown significantly increased mitochondrial OCR. (*F*) Graphical representation of glycolytic and CO_2-derived proton production rates in the control and HIF-1α knockdown cells. (*G*) FCCP treatment at 400, 800, and 1000nM significantly increased the total OCR by NP cells. All quantitative data are represented as mean ± SE, $n = 3$ independent biological replicates with 4 technical replicates per biological replicate, $^{*}p < 0.05$, $^{**}p < 0.01$. mpH = milli pH unit; PPR = proton production rate.

Given that we determined a large portion of extracellular proton production is from CO_2 hydration, we hypothesize that NP cells do in fact utilize the TCA cycle to generate metabolic precursors, NADH, and generate CO_2 from this pathway. Our previous studies have shown that although NP cells do not rely on mitochondria for ATP production, they are capable of using the TCA cycle for fatty acid oxidation.[10] Moreover, they are not limited by availability of intermediates like α-ketoglutarate that are generated through TCA cycle.[5,40] In addition, CO_2 (and NADPH) could be generated from decarboxylation reactions in pentose phosphate pathway known to generate five-carbon sugars glucose-6-phosphate in the cytosol.

Given such prominent contribution of CO_2 hydration to extracellular proton generation, it was logical to investigate if membrane-associated and extracellularly-facing carbonic anhydrases CA9 and CA12 are expressed in NP cells. These are the

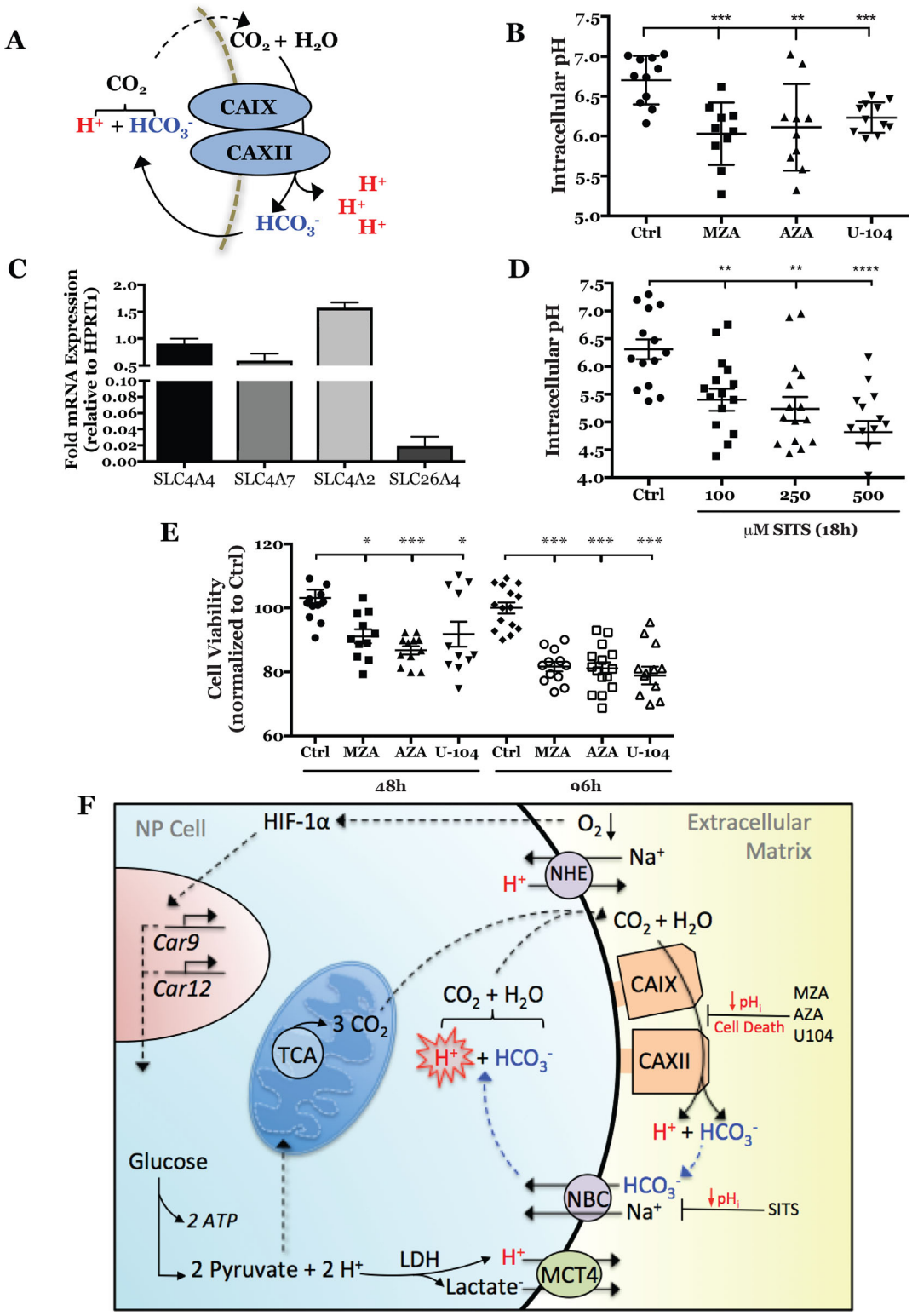

Fig. 9. Inhibition of CA9/12 causes a significant decrease in intracellular pH by blocking the generation of recycled bicarbonate. (*A*) Schematic of extracellular HCO_3^- generation and its intracellular recycling. (*B*) Intracellular pH significantly decreased after CA inhibition ($n = 3$; 3 to 4 technical replicates each). (*C*) qRT-PCR results showing expression of bicarbonate transporters in rat NP cells. (*D*) Intracellular pH significantly decreased after SITS treatment for 18 hours under hypoxia ($n = 4$; 3 technical replicates each). (*E*) Treatment of rat NP cells with MZA (500nM), AZA (500nM), and U-104 (2μM) for 48 and 96 hours in hypoxia significantly decreased cell viability. Data are represented as mean ± SE, $n \geq 3$ biological replicates, 3 to 6 technical replicates per biological replicate, $^{*}p < 0.05$, $^{**}p < 0.01$, $^{***}p < 0.001$. (*F*) Schematic of the proposed model of intracellular pH regulation through HCO_3^- recycling by the HIF-1α–carbonic anhydrase axis in NP cells.

only isoforms of the CA family that have been shown to be hypoxia-inducible in other cell types.[29–31] Although their in vivo expression is restricted to few adult tissues,[32,33,54] our results clearly showed robust expression of both isoforms in adult rat NP tissue. Our results also highlighted a positive relationship between hypoxia and their mRNA stability and expression. Because HIF-1 is a major regulator of hypoxic response in NP cells, and because of the known dependency of CA9 and CA12 on HIF-1 pathway, we determined if such a relationship exists in NP cells. Bioinformatic analyses showed that the proximal promoters of Car9 and Car12 contain three putative HRE regions, of which one HRE region in Car9 and two HRE regions in Car12 are conserved between rat and human promoters, suggesting that these regions could be important in regulation. Confirmation for this hypothesis was forthcoming from results of ChIP analysis, which clearly showed HIF-1α binding to the conserved HRE region (+1/+8 bp) at the Car9 transcription start site in rat NP cells. These results are in agreement with an earlier study that showed HIF-1α binding to a corresponding HRE in the human CA9 promoter.[55] Additionally, hypoxic enrichment of HIF-1α binding to the conserved HRE region (–91/–123 bp) closest to the transcription start site in the rat Car12 promoter suggested that these binding sites may play an important role in HIF-1α–dependent regulation of CA9 and CA12 in the NP. Taken together, our results suggested that, under hypoxia, both posttranscriptional regulation and HIF-1α binding to HREs contributed to Car9/12 mRNA stability and directly or indirectly to their expression in NP cells.

Notably, dependency of CA9 and CA12 on HIF-1α was evident from both in vitro and in vivo gain of function and loss of function approaches. First, we showed that stabilization of HIF-1α in normoxia upregulated Car12 mRNA expression; however, the inductive effect on Car9 was smaller. Considering that ChIP results showed similar HIF-1α binding to the Car9 promoter in normoxia and hypoxia, it is plausible that the expression of CA9 under normoxia is saturated. Alternatively, this may suggest requirement of hypoxia-specific co-activator/s for induction of CA9. Supporting gain-of-function experiments, stable silencing of HIF-1α in vitro resulted in a significant decrease in CA9 and CA12 mRNA and protein expression irrespective of oxemic tension, establishing a positive relationship between HIF-1α signaling and CA9/12 expression. Importantly, decreased expression of CAIX and CAXII in NP of mice with NP-specific deletion of HIF-1α provided, for the first time, conclusive in vivo evidence that CA9 and CA12 are transcriptional targets of HIF-1α in this hypoxic tissue.

Relevant to NP cell function, our studies showed that inhibition of CA9 and CA12 led to decreased ECAR and OCR that was not associated with changes in glycolytic flux or mitochondrial function. Our results suggest that CA inhibition has no effect on select pathways regulating or regulated by glycolytic flux, regardless of the HCO_3^- buffering capacity of the experimental setup. For example, HIF-1α transcriptional activity, expression of membrane-associated lactate exporters (MCT4), and extracellular lactate concentrations were not significantly altered upon CA inhibition. Similarly, catalytic inhibition of CA9 and CA12 lead to a decreased oxygen consumption rate that was not correlated with any decrease in mitochondrial respiration or functional dysregulation as measured by oxidoreductase activity. Together, these results showed that effect of CA inhibition on ECAR was independent of glycolysis but relied on abrogation of extracellular proton production from carbonic-anhydrase mediated CO_2 hydration; likewise, decreases in OCR were due to changes in non-mitochondrial pathways of O_2 consumption. Noteworthy this mode of action was different than when HIF-1α was silenced, which resulted in decreased glycolytic proton production and increased CO_2-dependent proton production, likely by increasing rates of TCA cycle production. This result further implicates HIF-1α as the gatekeeper of mitochondrial function and activity in the NP cell. Although it is important to note that healthy NP cells have non-mitochondrial oxygen consumption, the mechanism or purpose of this utilization has not been elucidated in this study and requires further investigation.

Our functional assays confirm that CO_2 hydration catalyzed by CA9 and CA12 produces HCO_3^- and H^+ ions in the pericellular space of NP cells. These HCO_3^- ions are then shuttled into the cytosol by NBCs to buffer pH_i, in a reaction that regenerates CO_2 and H_2O inside the NP cell. This model of HCO_3^- recycling is supported by our findings that clearly showed decreased pH_i in NP cells following both CA9/12 or NBC inhibition using specific pharmacological agents.

It must be appreciated that the exact molecular players of the HCO_3^- transport metabolon in NP cells are unknown. This term was coined to describe the coordinated efforts of common pH-regulating proteins to transport HCO_3^- across the cell membrane, and was first detected by the interactions between CAII (Carbonic Anhydrase II) and AE1 (Anion Exchanger 1), a Cl^-/HCO_3^- exchanger in erythrocytes.[56] Investigations into membrane associated HCO_3^- transporters in the disc, however, are seldom. In the present study, however, we confirmed the expression of four membrane-associated bicarbonate transporters, namely NBCe1, NBCn1, AE2, and Pendrin, a rare enzyme commonly associated with thyroid pathology.[34] Although these results are interesting, further research into the coordinated HCO_3^- transporters that work in tandem with CA9/12 is essential for a thorough understanding of pH regulation in the NP. Concerning the fate of extracellular H^+ units produced along with HCO_3^- by CA9 and CA12 catalytic reaction, we hypothesize that they will only be transiently available in the pericellular space and will be secreted out of the disc or, alternatively, could be used as a form of energy currency. In this sense, extracellularly-facing CA9 and CA12 may act as H^+ donors for nearby membrane associated co-transporters (such as MCTs) that also function in the complex network of pH sensors.[57,58]

Our results suggested that in NP cells, extracellularly-facing and membrane-associated CA9 and CA12 isoforms serve as a critical line of defense against accumulation of intracellular H^+. Because plasma-membrane H^+ extrusion systems alone may not be sufficient in maintaining physiological pH_i in NP cells,[11] and the otherwise ubiquitous CA2 isozyme is not as highly expressed (GEO Accession #GSE86552),[25] generation of pericellular HCO_3^- ions by CA9/12 assumes high significance. This mechanism of pH regulation is both essential and unique to NP cells, which are prone to high intracellular lactate and H^+ concentrations. Without the essential activity of CA9 and CA12, NP cells will have compromised survival in the hypoxic disc environment, a notion supported by our viability measurements following long-term CA inhibition. In summary, the HIF-1α–carbonic anhydrase axis is critical for NP cell survival and alteration in their expression and activity will compromise tissue function and exacerbate the diseased state.

Disclosures

All authors state that they have no conflicts of interest.

Acknowledgments

This work is supported by grants from the NIH (National Institute of Arthritis and Musculoskeletal and Skin Diseases [NIAMS] AR055655 and AR064733 to MVR). ES is supported by NIAMS grant T32 AR052273.

Authors' roles: ESS, ES, IMS, and MVR conceived the study. ESS, ZRS, ELS, and CM conducted the experiments, analyzed data, and wrote the manuscript. IMS designed the study, wrote the manuscript, and secured funding. MVR designed experiments, interpreted results, secured funding, and wrote the manuscript. All authors reviewed the results and approved the final version of the manuscript.

References

1. Katz JN. Lumbar disc disorders and low-back pain: socioeconomic factors and consequences. J Bone Joint Surg Am. 2006;88 Suppl 2:21–4.
2. Murray CJ, Atkinson C, Bhalla K, et al.; U.S. Burden of Disease Collaborators. The state of US Health, 1990-2010: burden of diseases, injuries, and risk factors. JAMA. 2013;310:591–608.
3. Johnson ZI, Shapiro IM, Risbud MV. Extracellular osmolarity regulates matrix homeostasis in the intervertebral disc and articular cartilage: evolving role of TonEBP. Matrix Biol. 2014;40:10–6.
4. Risbud MV, Guttapalli A, Stokes DG, et al. Nucleus pulposus cells express HIF-1 alpha under normoxic culture conditions: a metabolic adaptation to the intervertebral disc microenvironment. J Cell Biochem. 2006;98:152–9.
5. Fujita N, Chiba K, Shapiro IM, Risbud MV. HIF-1alpha and HIF-2alpha degradation is differentially regulated in nucleus pulposus cells of the intervertebral disc. J Bone Miner Res. 2012;27:401–12.
6. Gruber HE, Ashraf N, Kilburn J, et al. Vertebral endplate architecture and vascularization: application of micro-computerized tomography, a vascular tracer, and immunocytochemistry in analyses of disc degeneration in the aging sand rat. Spine (Phila Pa 1976). 2005;30:2593–600.
7. Bibby SR, Jones DA, Ripley RM, Urban JP. Metabolism of the intervertebral disc: effects of low levels of oxygen, glucose, and pH on rates of energy metabolism of bovine nucleus pulposus cells. Spine (Phila Pa 1976). 2005;30:487–96.
8. Urban JP, Smith S, Fairbank JC. Nutrition of the intervertebral disc. Spine (Phila Pa 1976). 2004;29:2700–9.
9. Bartels EM, Fairbank JC, Winlove CP, Urban JP. Oxygen and lactate concentrations measured in vivo in the intervertebral discs of patients with scoliosis and back pain. Spine (Phila Pa 1976). 1998;23:1–7; discussion 8.
10. Agrawal A, Guttapalli A, Narayan S, Albert TJ, Shapiro IM, Risbud MV. Normoxic stabilization of HIF-1alpha drives glycolytic metabolism and regulates aggrecan gene expression in nucleus pulposus cells of the rat intervertebral disk. Am J Physiol Cell Physiol. 2007;293: C621–31.
11. Razaq S, Urban JP, Wilkins RJ. Regulation of intracellular pH by bovine intervertebral disc cells. Cell Physiol Biochem. 2000;10:109–15.
12. Diamant B, Karlsson J, Nachemson A. Correlation between lactate levels and pH in discs of patients with lumbar rhizopathies. Experientia. 1968;24:1195–6.
13. Nachemson A. Intradiscal measurements of pH in patients with lumbar rhizopathies. Acta Orthop Scand. 1969;40:23–42.
14. Ohshima H, Urban JP. The effect of lactate and pH on proteoglycan and protein synthesis rates in the intervertebral disc. Spine (Phila Pa 1976). 1992;17:1079–82.
15. Razaq S, Wilkins RJ, Urban JP. The effect of extracellular pH on matrix turnover by cells of the bovine nucleus pulposus. Eur Spine J. 2003;12:341–9.
16. Gilbert HT, Hodson N, Baird P, Richardson SM, Hoyland JA. Acidic pH promotes intervertebral disc degeneration: acid-sensing ion channel -3 as a potential therapeutic target. Sci Rep. 2016;6:37360.
17. Swietach P, Vaughan-Jones RD, Harris AL. Regulation of tumor pH and the role of carbonic anhydrase 9. Cancer Metastasis Rev. 2007;26:299–310.
18. Swietach P, Hulikova A, Vaughan-Jones RD, Harris AL. New insights into the physiological role of carbonic anhydrase IX in tumour pH regulation. Oncogene. 2010;29:6509–21.
19. McIntyre A, Hulikova A, Ledaki I, et al. Disrupting hypoxia-induced bicarbonate transport acidifies tumor cells and suppresses tumor growth. Cancer Res. 2016;76:3744–55.
20. McMurtrie HL, Cleary HJ, Alvarez BV, et al. The bicarbonate transport metabolon. J. Enzyme Inhib Med Chem. 2004;19:231–6.
21. Parks SK, Chiche J, Pouysségur J. Disrupting proton dynamics and energy metabolism for cancer therapy. Nat Rev Cancer. 2013;13:611–23.
22. Casey JR, Grinstein S, Orlowski J. Sensors and regulators of intracellular pH. Nat Rev Mol Cell Biol. 2010;11:50–61.
23. Maren TH. Carbonic anhydrase: chemistry, physiology, and inhibition. Physiol Rev. 1967;47:595–781.
24. Mookerjee SA, Goncalves RL, Gerencser AA, Nicholls DG, Brand MD. The contributions of respiration and glycolysis to extracellular acid production. Biochim Biophys Acta. 2015;1847:171–81.
25. Johnson ZI, Shapiro IM, Risbud MV. RNA sequencing reveals a role of TonEBP in regulation of pro-inflammatory genes in response to hyperosmolarity in healthy nucleus pulposus cells: a homeostatic response? J Biol Chem. 2016;291(52):26686–97. DOI:10.1074/jbc.M116.757732.
26. Markova DZ, Kepler CK, Addya S, et al. An organ culture system to model early degenerative changes of the intervertebral disc II: profiling global gene expression changes. Arthritis Res Ther. 2013;15:R121.
27. Kao TH, Peng YJ, Tsou HK, Salter DM, Lee HS. Nerve growth factor promotes expression of novel genes in intervertebral disc cells that regulate tissue degradation: laboratory investigation. J Neurosurg Spine. 2014;21:653–61.
28. Miyamoto T, Muneta T, Tabuchi T, et al. Intradiscal transplantation of synovial mesenchymal stem cells prevents intervertebral disc degeneration through suppression of matrix metalloproteinase-related genes in nucleus pulposus cells in rabbits. Arthritis Res Ther. 2010;12:R206.
29. Chiche J, Ilc K, Laferrière J, et al. Hypoxia-inducible carbonic anhydrase IX and XII promote tumor cell growth by counteracting acidosis through the regulation of the intracellular pH. Cancer Res. 2009;69:358–68.
30. Wykoff CC, Beasley NJ, Watson PH, et al. Hypoxia-inducible expression of tumor-associated carbonic anhydrases. Cancer Res. 2000;60(24):7075–83.
31. Švastová E, Hulíková A, Rafajová M, et al. Hypoxia activates the capacity of tumor-associated carbonic anhydrase IX to acidify extracellular pH. FEBS Lett. 2004;577:439–45.
32. Kallio H, Pastorekova S, Pastorek J, et al. Expression of carbonic anhydrases IX and XII during mouse embryonic development. BMC Dev Biol. 2006;6:22.
33. Kivelä A, Parkkila S, Saarnio J, et al. Expression of a novel transmembrane carbonic anhydrase isozyme XII in normal human gut and colorectal tumors. Am J Pathol. 2000;156:577–84.
34. Cordat E, Casey JR. Bicarbonate transport in cell physiology and disease. Biochem J. 2009;417:423–39.
35. Boron WF, Chen L, Parker MD. Modular structure of sodium-coupled bicarbonate transporters. J Exp Biol. 2009;212:1697–706.
36. Schoepflin ZR, Shapiro IM, Risbud MV. Class I and IIa HDACs mediate HIF-1α stability through PHD2-dependent mechanism while HDAC6, a class IIb member, promotes HIF-1α transcriptional activity in nucleus pulposus cells of the intervertebral disc. J Bone Miner Res. 2016;31:1287–99. DOI:10.1002/jbmr.2787.
37. Gogate SS, Fujita N, Skubutyte R, Shapiro IM, Risbud MV. Tonicity enhancer binding protein (TonEBP) and hypoxia-inducible factor (HIF) coordinate heat shock protein 70 (Hsp70) expression in hypoxic nucleus pulposus cells: role of Hsp70 in HIF-1α degradation. J Bone Miner Res. 2012;27:1106–17.
38. Tran CM, Fujita N, Huang BL, et al. Hypoxia-inducible factor (HIF)-1alpha and CCN2 form a regulatory circuit in hypoxic nucleus

pulposus cells: CCN2 suppresses HIF-1alpha level and transcriptional activity. J Biol Chem. 2013;288:12654–66.

39. Suyama K, Silagi ES, Choi H, et al. Circadian factors BMAL1 and RORα control HIF-1α transcriptional activity in nucleus pulposus cells: implications in maintenance of intervertebral disc health. Oncotarget. 2016;7:23056–71.
40. Fujita N, Gogate SS, Chiba K, Toyama Y, Shapiro IM, Risbud MV. Prolyl hydroxylase 3 (PHD3) modulates catabolic effects of tumor necrosis factor-alpha (TNF-α) on cells of the nucleus pulposus through co-activation of nuclear factor kappa-B (NF-κB)/p65 signaling. J Biol Chem. 2012;287:39942–53.
41. Power KA, Grad S, Rutges JP, et al. Identification of cell surface-specific markers to target human nucleus pulposus cells: expression of carbonic anhydrase XII varies with age and degeneration. Arthritis Rheum. 2011;63:3876–86.
42. Chen S, Fang XQ, Wang Q, et al. PHD/HIF-1 upregulates CA12 to protect against degenerative disc disease: a human sample, in vitro and ex vivo study. Lab Invest. 2016;96:561–9. DOI:10.1038/labinvest.2016.32.
43. Pacchiano F, Carta F, McDonald PC, et al. Ureido-substituted benzenesulfonamides potently inhibit carbonic anhydrase IX and show antimetastatic activity in a model of breast cancer metastasis. J Med Chem. 2011;54:1896–902.
44. Csordás G, Golenár T, Seifert EL, et al. MICU1 controls both the threshold and cooperative activation of the mitochondrial Ca2+ uniporter. Cell Metab. 2013;17:976–87.
45. Risbud MV, Schoepflin ZR, Mwale F, et al. Defining the phenotype of young healthy nucleus pulposus cells: recommendations of the Spine Research Interest Group at the 2014 annual ORS meeting. J Orthop Res. 2015;33:283–93.
46. Merceron C, Mangiavini L, Robling A, et al. Loss of HIF-1α in the notochord results in cell death and complete disappearance of the nucleus pulposus. PLoS One. 2014;9(10):e110768. DOI:10.1371/journal.pone.0110768.
47. Mathelier A, Fornes O, Arenillas DJ, et al. JASPAR 2016: a major expansion and update of the open-access database of transcription factor binding profiles. Nucleic Acids Res. 2016;44(D1):D110–5. DOI:10.1093/nar/gkv1176.
48. van der Windt GJW, Chang CH, Pearce EL. Measuring bioenergetics in T cells using a Seahorse Extracellular Flux Analyzer. Curr Protoc Immunol. 2016;113:16B.1–16B.14. DOI:10.1002/0471142735.im0316bs113.
49. Tan B, Xiao H, Li F, Zeng L, Yin Y. The profiles of mitochondrial respiration and glycolysis using extracellular flux analysis in porcine enterocyte IPEC-J2. Animal Nutrition. 2015;1:239–43. DOI:10.1016/j.aninu.2015.08.004.
50. Supuran CT. Carbonic anhydrase inhibitors. Bioorg Med Chem Lett. 2010;20:3467–74.
51. Harju AK, Bootorabi F, Kuuslahti M, Supuran CT, Parkkila S. Carbonic anhydrase III: a neglected isozyme is stepping into the limelight. J Enzyme Inhib Med Chem. 2012;28:1–9.
52. Dimmer KS, Friedrich B, Lang F, Deitmer JW, Bröer S. The low-affinity monocarboxylate transporter MCT4 is adapted to the export of lactate in highly glycolytic cells. Biochem J. 2000;350(Pt 1):219–27.
53. Morgan PE, Pastorekova S, Stuart-Tilley AK, Alper SL, Casey JR. Interactions of transmembrane carbonic anhydrase, CAIX, with bicarbonate transporters. Am J Physiol Cell Physiol. 2007;293:C738–48.
54. Türeci O, Sahin U, Vollmar E, et al. Human carbonic anhydrase XII: cDNA cloning, expression, and chromosomal localization of a carbonic anhydrase gene that is overexpressed in some renal cell cancers. Proc Natl Acad Sci U S A. 1998;95:7608–13.
55. Kaluz S, Kaluzová M, Liao SY, Lerman M, Stanbridge EJ. Transcriptional control of the tumor- and hypoxia-marker carbonic anhydrase 9: a one transcription factor (HIF-1) show? Biochim Biophys Acta. 2009;1795:162–72.
56. Vince JW, Reithmeier RA. Carbonic anhydrase II binds to the carboxyl terminus of human band 3, the erythrocyte $C1^-/HCO_3^-$ exchanger. J Biol Chem. 1998;273, 28430–7.
57. Jamali S, Klier M, Ames S, et al. Hypoxia-induced carbonic anhydrase IX facilitates lactate flux in human breast cancer cells by non-catalytic function. Sci Rep. 2015;5:13605.
58. Stridh MH, Alt MD, Wittmann S, et al. Lactate flux in astrocytes is enhanced by a non-catalytic action of carbonic anhydrase II. J Physiol. 2012;590:2333–51.